AD 296 167

AFCRL-62-1073

FURTHER STUDIES OF NUMERICAL ERRORS IN THE INTEGRATION OF BAROTROPIC FLOW ON A SPHERICAL GRID

by
W. LAWRENCE GATES
and
CHRISTOPHER A. RIEGEL
University of California, Los Angeles

FINAL REPORT
1 July 1960 - 31 December 1962
Project 8628
Task 862803

DYNAMICAL WEATHER PREDICTION PROJECT
Department of Meteorology
31 December, 1962

The research described in this report has been sponsored by the Geophysics Research Directorate of the Air Force Cambridge Research Laboratories, Office of Aerospace Research (USAF), under Contract No. AF 19 (604)-6149.

Requests for additional copies by Agencies of the Department of Defense, their contractors, and other Government agencies should be directed to the:

ARMED SERVICES TECHNICAL INFORMATION AGENCY
ARLINGTON HALL STATION
ARLINGTON 12, VIRGINIA

Department of Defense contractors must be established for ASTIA services or have their 'need-to-know' certified by the cognizant military agency of their project or contract.

All other persons and organizations should apply to the:

U. S. DEPARTMENT OF COMMERCE
OFFICE OF TECHNICAL SERVICES
WASHINGTON 25, D.C.

FURTHER STUDIES OF NUMERICAL ERRORS IN THE INTEGRATION OF BAROTROPIC FLOW ON A SPHERICAL GRID

by

W. Lawrence Gates

and

Christopher A. Riegel

University of California, Los Angeles

FINAL REPORT

1 July 1960 - 31 December 1962

Project 8628

Task 862803

DYNAMICAL WEATHER PREDICTION PROJECT

Department of Meteorology

31 December 1962

The research described in this report has been sponsored by the Geophysics Research Directorate of the Air Force Cambridge Research Laboratories, Office of Aerospace Research (USAF), under Contract No. AF 19(604)-6149.

PREFACE

The research described in this report represents the continuation of an extended investigation of numerical errors in dynamical weather prediction, initiated and performed under the previous contracts AF 19(604)-3886 and AF 19(604)-4965 during the period 1 July 1958-30 June 1960.

The project personnel during the present contractual period 1 July 1960-31 December 1962 has consisted of the following:

Miss L. Fujinaka, 13 June 1960 - 30 September 1960

Mr. J. R. Hammond, 9 September 1960 - 15 June 1962

Mr. E. G. Lucero, 25 January 1962 - 25 May 1962

Miss M. H. Oberländer, 1 July 1960 - 31 December 1962

Mr. C. A. Riegel, 1 July 1960 - 30 September 1960

Mr. F. J. Winninghoff, 9 September 1960 - 30 June 1961

Employed on an occasional hourly basis during the contractual period were Miss B. Peeler and Miss M. Zenderman.

During the contractual period, four Scientific Reports were issued:

1. Static stability measures in the atmosphere, by W. Lawrence Gates. Scientific Report No. 3, 31 October 1960, 22 pp. (This report was prepared under the previous Contract AF 19(604)-4965). Published under the same title in J. Meteor., 18: 526-533 (1961).

2. Preliminary study of numerical errors in the integration of barotropic flow on a spherical grid, by W. Lawrence Gates and Christopher A. Riegel. Scientific Report No. 4, 15 March 1961, 46 pp. Published under the same title in J. Geophys. Res. 67: 773-784 (1962).

3. The propagation of error in numerical integration of the discrete vorticity equation, by W. Lawrence Gates. Scientific Report No. 6, 15 May 1962, 37 pp.

4. The effect of finite differences on the growth rates of unstable waves in a simple baroclinic model, by Christopher A. Riegel. Scientific Report No. 7, 1 October 1962, 24 pp.

W. Lawrence Gates
Project Director

ABSTRACT

Using a spherical finite-difference grid system covering the hemisphere, numerical solutions of the non-divergent barotropic vorticity equation have been obtained for periods up to 10 days by relaxation methods. In the case of analytic initial conditions, the solutions are sensitive to abrupt changes of the longitudinal mesh size in the regions of appreciable amplitude of the streamfunction tendency. A doubling of the longitudinal mesh size from 5 to 10 deg at 45°N produces a progressive tearing or shearing in the streamfunction which is quite noticeable at 10 days. When the grid variation is removed to 70°N, however, the solutions at 10 days are free of this defect, although exhibiting the expected phase lag relative to the analytic solution. When applied to hemispherical barotropic prediction with actual 500 mb data, this spherical grid scheme appears to perform as satisfactorily as do conventional (rectangular) grid formulations.

TABLE OF CONTENTS

1. Introduction.

In an earlier study (Gates and Riegel, 1962) the problem of numerically integrating the barotropic vorticity equation on a spherical finite-difference grid was considered. By comparing the numerical solutions with analytic solutions for a simple harmonic initial condition, the dominant sole of the space truncation error was identified. It is the purpose of the present paper to extend these analytic-numerical comparisons to somewhat longer periods of integration, and to report on an improvement in the grid design as a result of these investigations.

It is sufficient here to recall that the barotropic vorticity equation for horizontal non-divergent flow may be written in the form

$$\frac{\partial \eta_s}{\partial t} = \frac{1}{r^2 \cos\phi}\left[\frac{\partial \eta_s}{\partial \lambda}\frac{\partial \psi}{\partial \phi} - \frac{\partial \eta_s}{\partial \phi}\frac{\partial \psi}{\partial \lambda}\right], \qquad (1)$$

with the vorticity given by

$$\eta_s = f + \frac{1}{r^2\cos\phi}\frac{\partial}{\partial \phi}\left(\cos\phi \frac{\partial \psi}{\partial \phi}\right) + \frac{1}{r^2\cos^2\phi}\frac{\partial^2 \psi}{\partial \lambda^2}. \qquad (2)$$

Here ψ is a streamfunction, r the radius of the assumed spherical earth, ϕ the latitude, and λ the longitude. This equation is approximated by the finite-difference equation

$$(h_1 - h_2)\left(\frac{\partial \psi}{\partial t}\right)_{ij+1} + (h_1 + h_2)\left(\frac{\partial \psi}{\partial t}\right)_{ij-1} + h_1^{-1}\left(\frac{\partial \psi}{\partial t}\right)_{i+mj} + h_1^{-1}\left(\frac{\partial \psi}{\partial t}\right)_{i-mj} - (2h_1 + 2h_1^{-1})\left(\frac{\partial \psi}{\partial t}\right)_{ij}$$

$$= \frac{1}{4}\left[(\eta_{i+mj} - \eta_{i-mj})(\psi_{ij+1} - \psi_{ij-1}) - (\eta_{ij+1} - \eta_{ij-1})(\psi_{i+mj} - \psi_{i-mj})\right], \qquad (3)$$

where

$$n_1 = m \Delta\lambda (\Delta\phi)^{-1} \cos\phi \quad , \tag{4}$$

$$n_2 = m \Delta\lambda (2)^{-1} \sin\phi \quad , \tag{5}$$

and where $\Delta\phi$ and $\Delta\lambda$ are the basic (5 deg) latitudinal and longitudinal mesh increments, respectively, with corresponding integer indicies i and j .

The details of this difference scheme, the treatment of the pole, and the method of numerical solution have been described earlier (Gates and Riegel, 1962). The distinguishing notion of this approach, however, is the identification of the points $i \pm m$ in (3) above as those at the neighboring points ± 5 deg long away (i.e., $m = 1$) for $0 \leq \phi \leq 45$N, and taking $m = 2$ for the latitudes 50-65N, $m = 3$ for 70N, $m = 4$ for 75N, $m = 6$ for 80N and $m = 12$ at 85 N. Equation (3) is itself, however, applied to each point of the basic 72 x 18 point gria, with the pole treated separately. In this fashion comparable grid resolution is maintained over a wide range of latitude without interpolation.

2. Extended numerical integrations.

In the previous study (Gates and Riegel, 1962) it was found that in the solution of (3) by the extrapolated Liebmann relaxation method, an overrelaxation coefficient $\alpha = 0.36$ and a streamfunction tendency residue tolerance of 0.07 percent of the maximum initial tendency were suitable values for the analytic case selected.

These numerical solutions have now been extended to 10 days (with time steps Δt = 1 hr), and are shown in a sixth part in Figs. 1-5. A sixth part of the associated streamfunction error fields are shown in Figs. 6-10 for this case of six symmetrical hemispheric waves moving eastward at 20 deg long per day without change of shape.

It may be noted that the waves retain their general initial configuration until approximately 6 days, and move at about 96 percent of the true wave speed. After this time, however, an increasingly serious distortion occurs, such that by 10 days the initial wave pattern is noticeably altered. Closer examination of Figs. 6-8 shows a steadily increasing streamfunction error field of the type to be expected from a persistent phase speed lag of the predicted versus the actual wave. Figs. 9 and 10, however, show a somewhat more rapid error growth, with a pronounced error asymmetry by 10 days. This distortion appears first near the latitude at which the effective longitudinal mesh size is first doubled, i.e., between 45N and 50N. Due to the increased truncation error the predicted wave speed to the north of this juncture is less than it is to the south, and this evidently introduces a fictitious "backward" tilt to the wave. This effect is here less noticeable at the higher latitudes (at which similar longitudinal mesh size changes occur)because of the somewhat smaller wave amplitude in these regions.

This characteristic wave distortion also occurred in the extended integrations with a doubled (10 deg) basic grid size, as shown in Figs. 11 and 12. The larger truncation error in this case, however, evidently masks the distortion so that it is less clearly displayed at 10 days than in the case of the 5 deg grid discussed above.

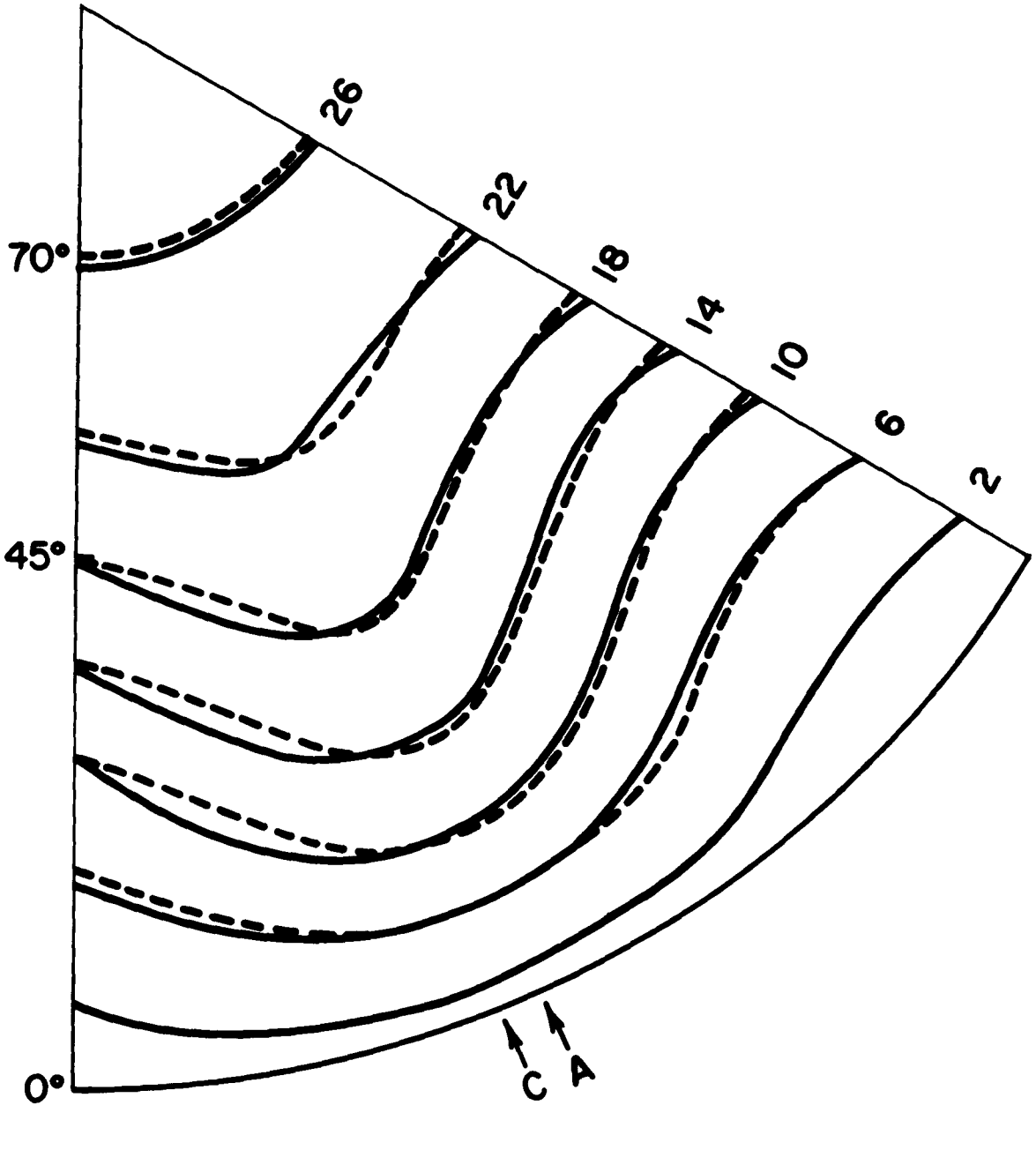

Figure 1. A sixth part of the computed stream function solution at t = 2 days with the original 5 deg grid, with α = 0.36, ϵ = 0.50 $m^2 sec^{-2}$, and Δt = 1 hr. The dashed lines are the corresponding analytic solution. The units are $10^7 m^2 sec^{-1}$, and the arrows "A" and "C" indicate the positions of the analytic and computed stream function troughs, respectively. All stream function values are negative.

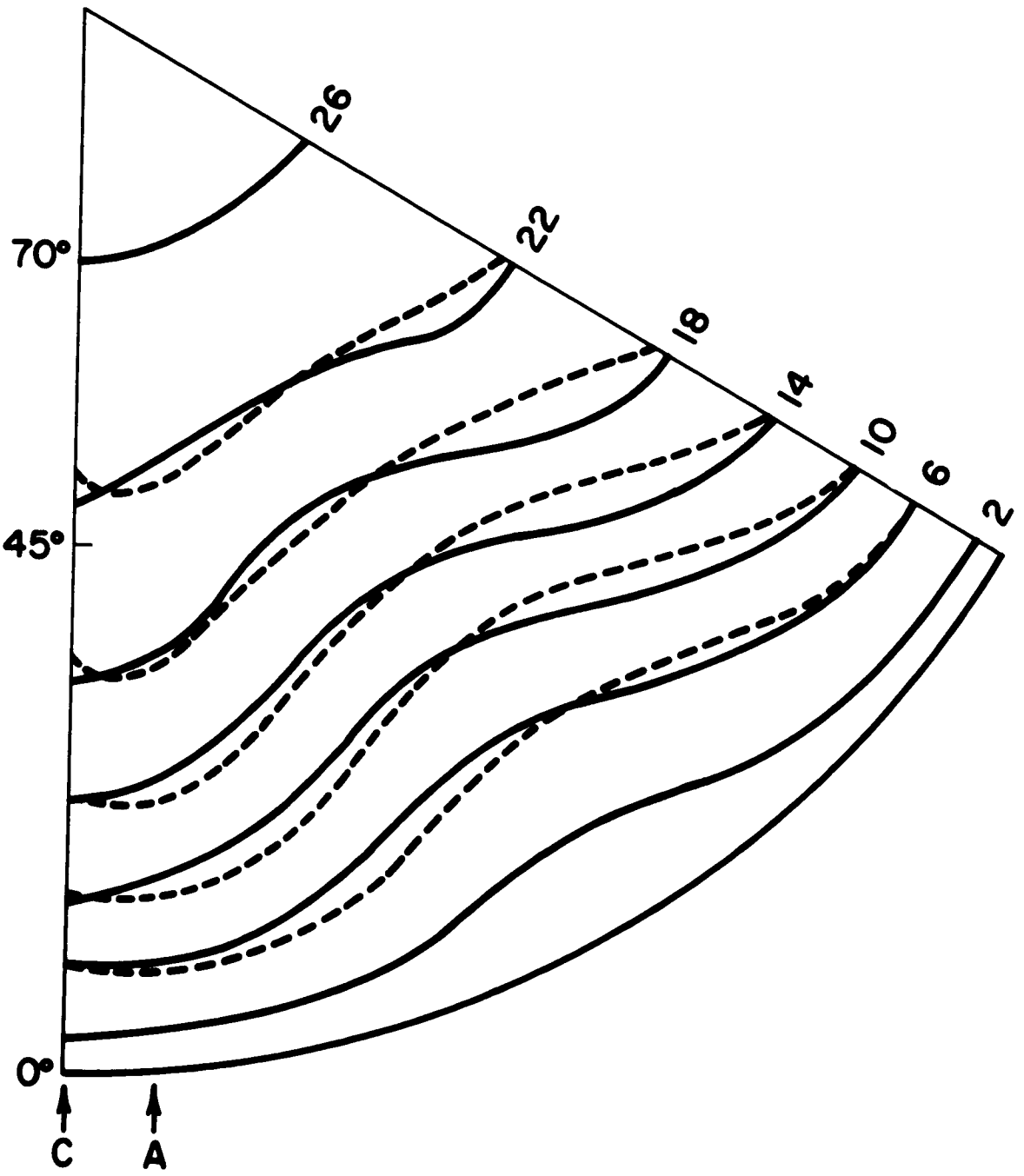

Figure 2. Same as fig. 1, but for t = 4 days.

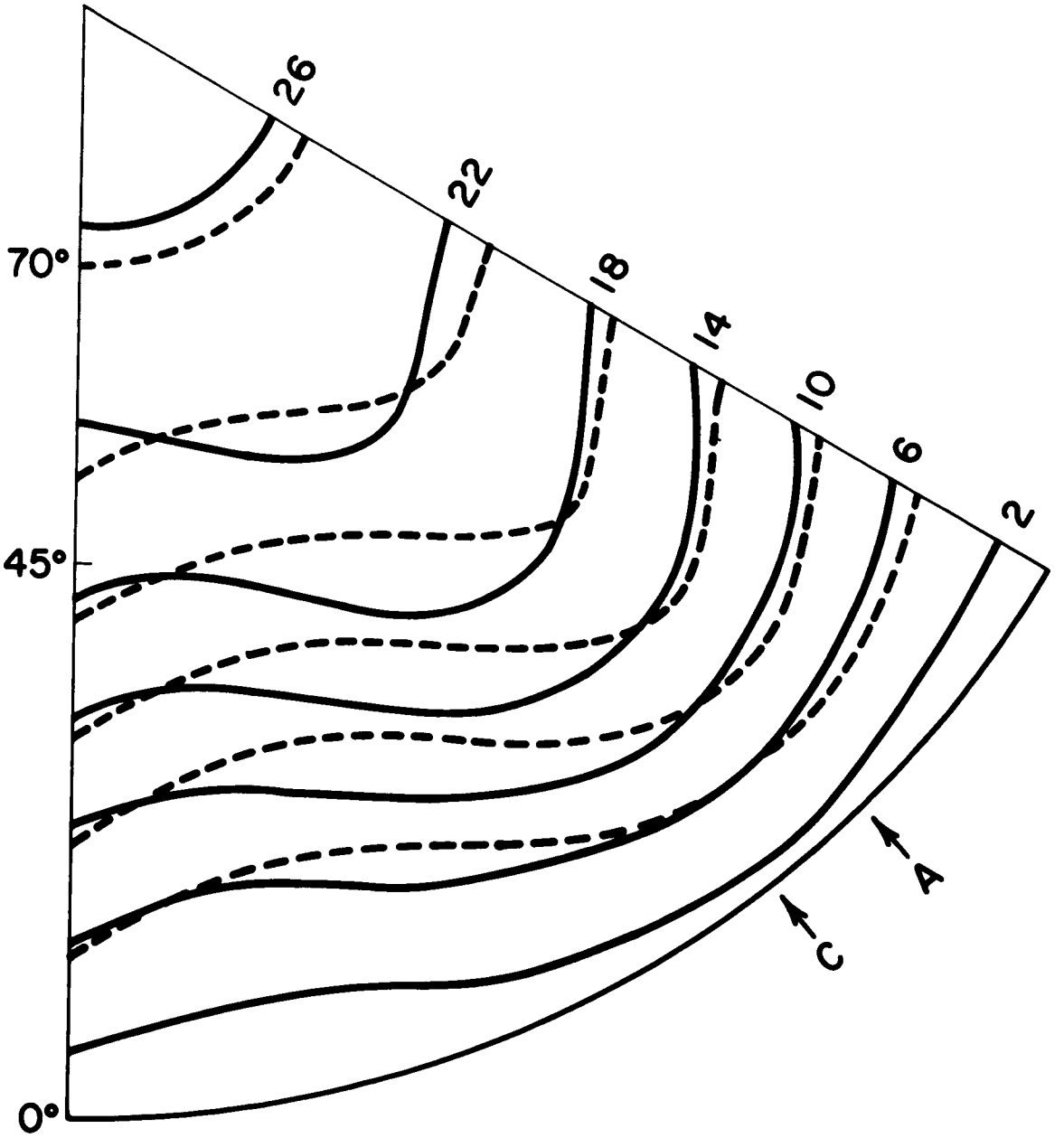

Figure 3. Same as fig. 1, but for t = 6 days.

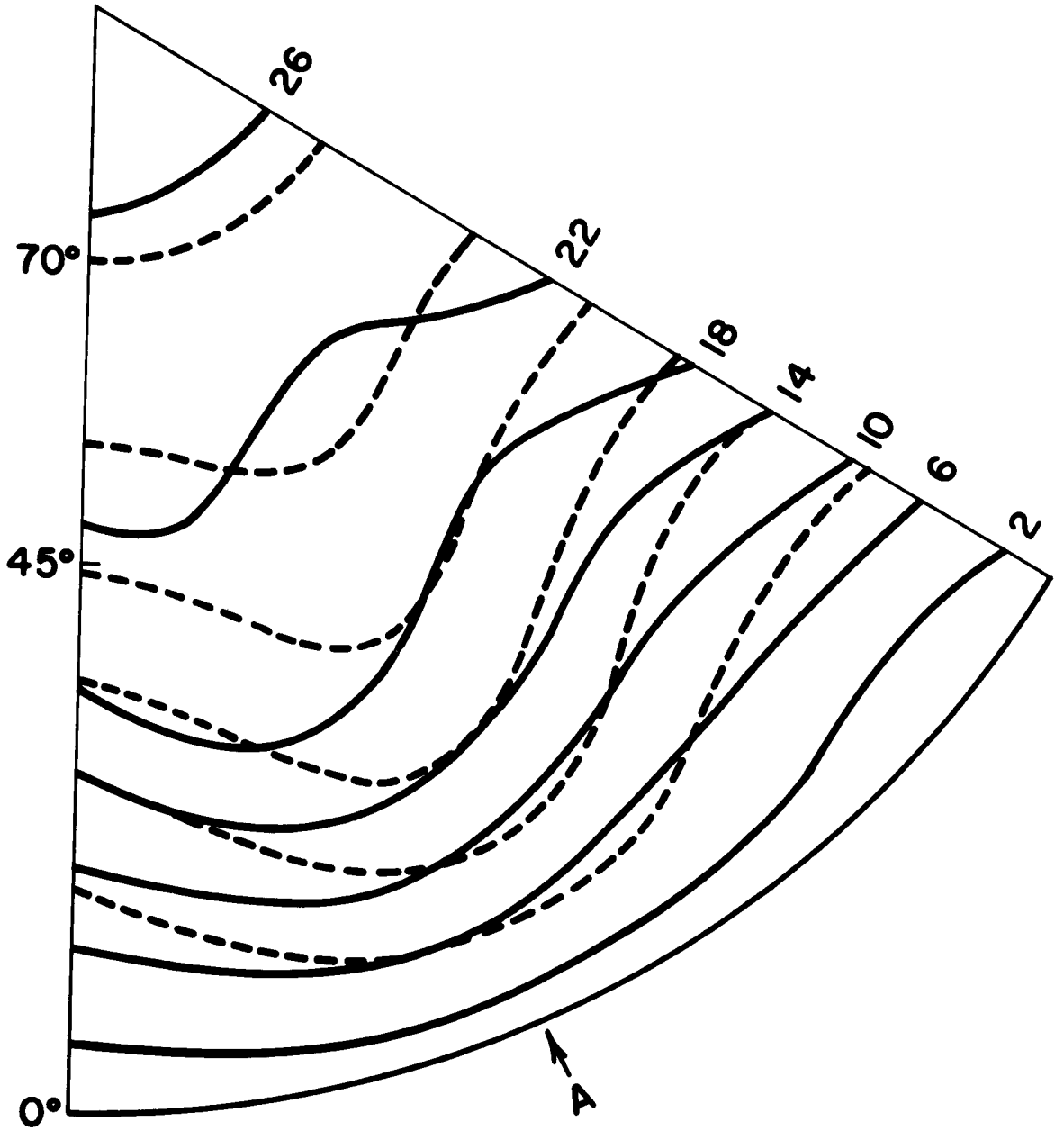

Figure 4. Same as fig. 1, but for t = 8 days.

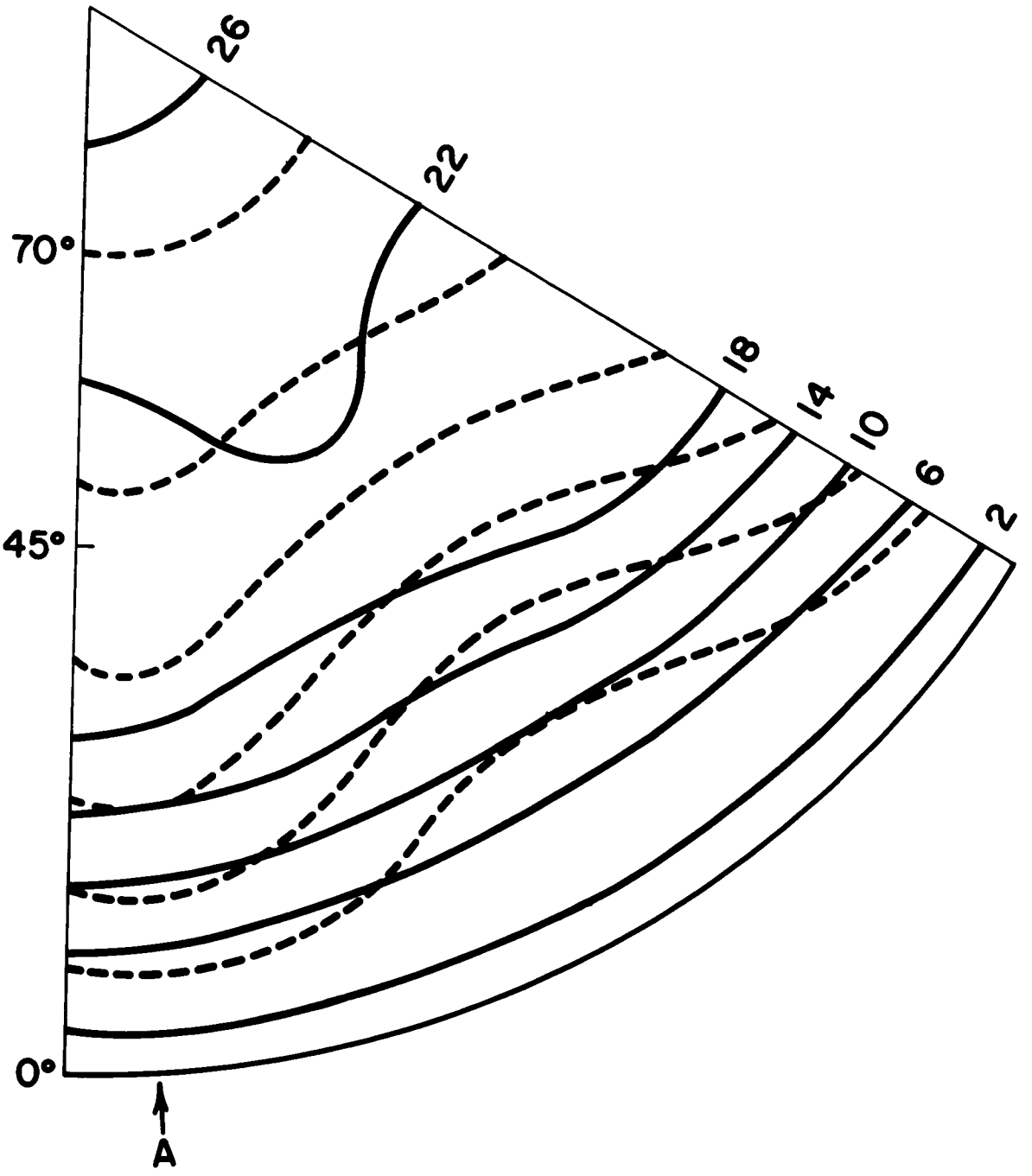

Figure 5. Same as fig. 1, but for t = 10 days.

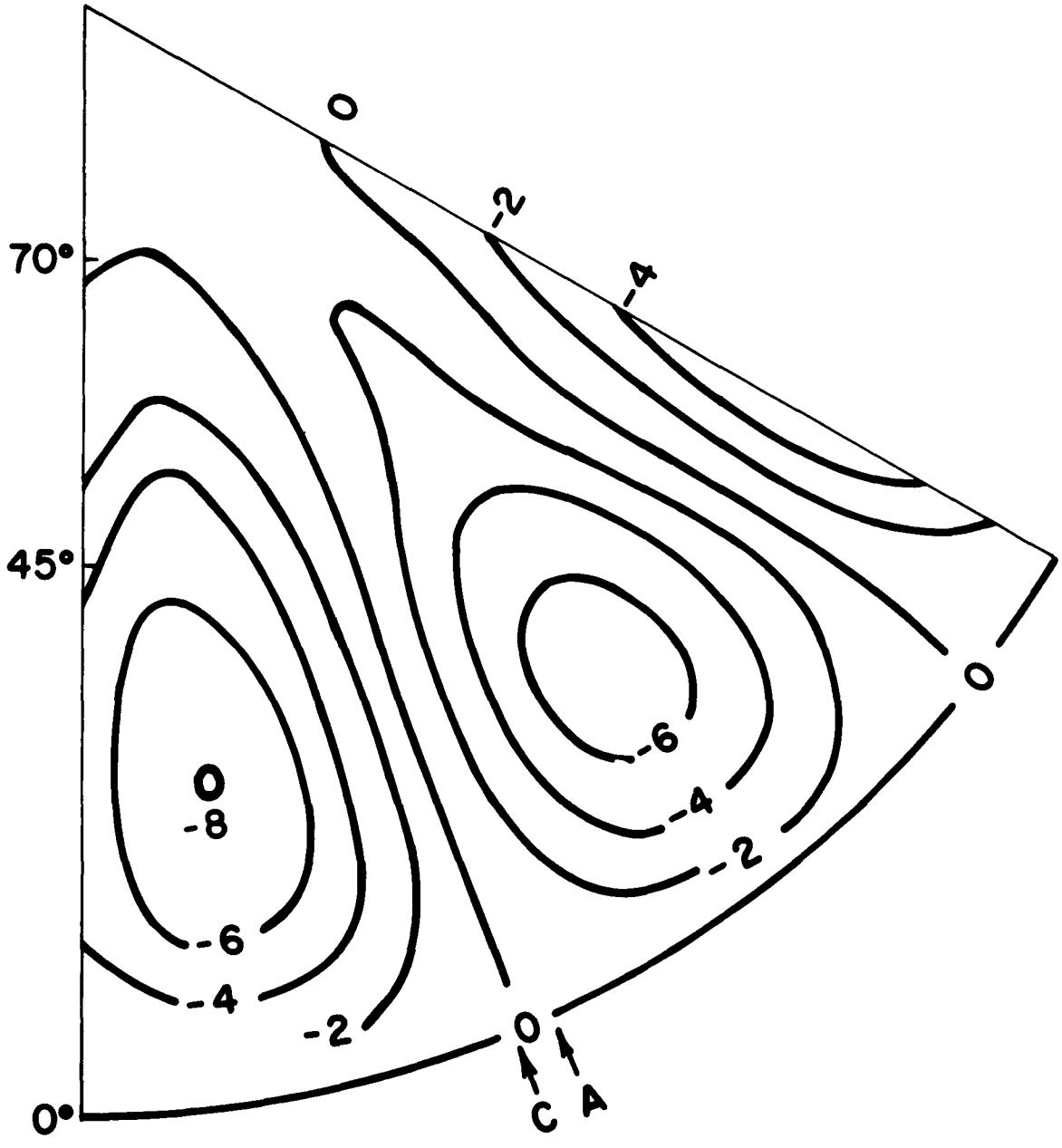

Figure 6. A sixth part of the error field of the computed stream function solution at t = 2 days with the original 5 deg grid. The units are $10^6 m^2 sec^{-1}$. See fig. 1.

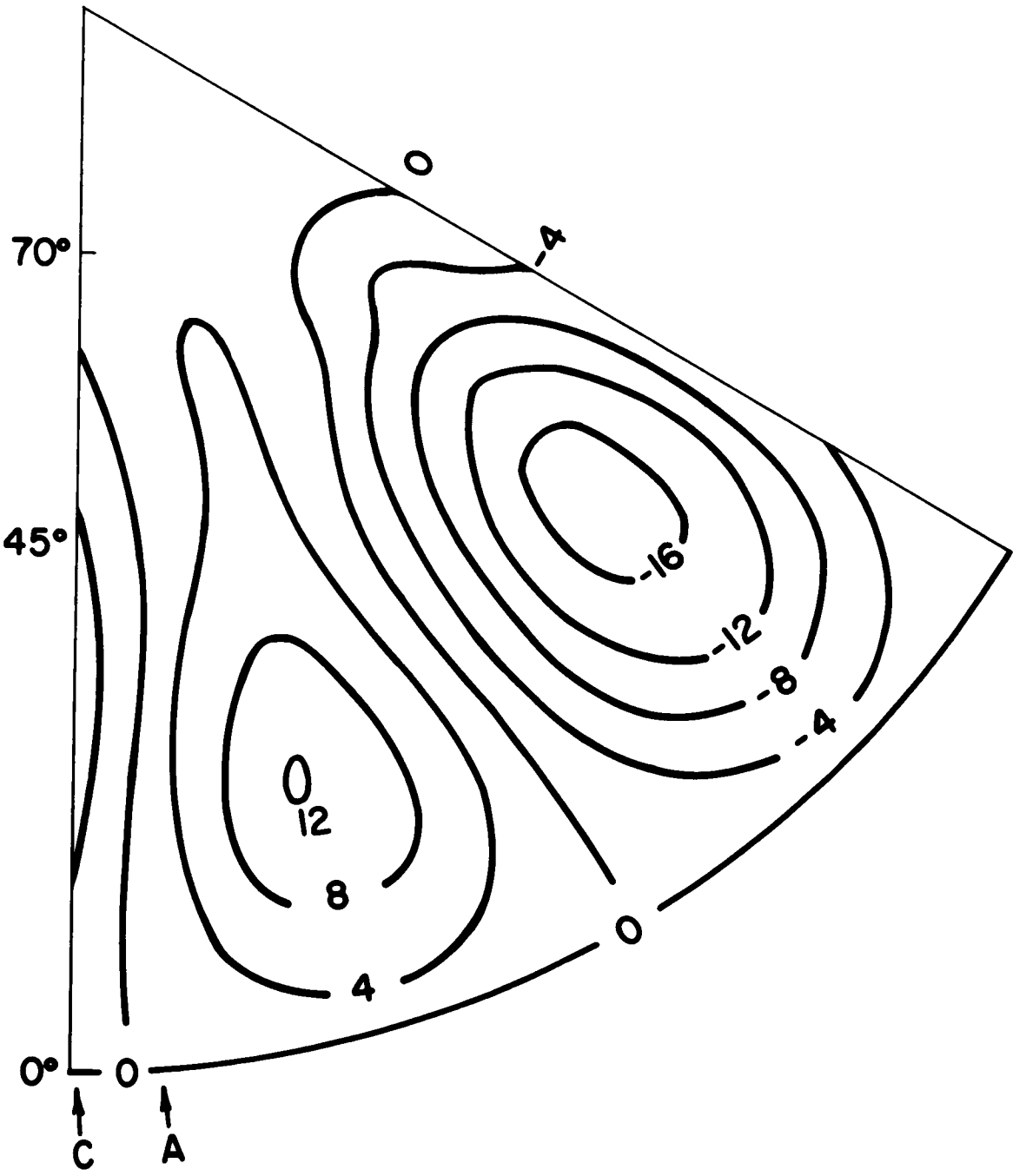

Figure 7. Same as fig. 6, but for t = 4 days.

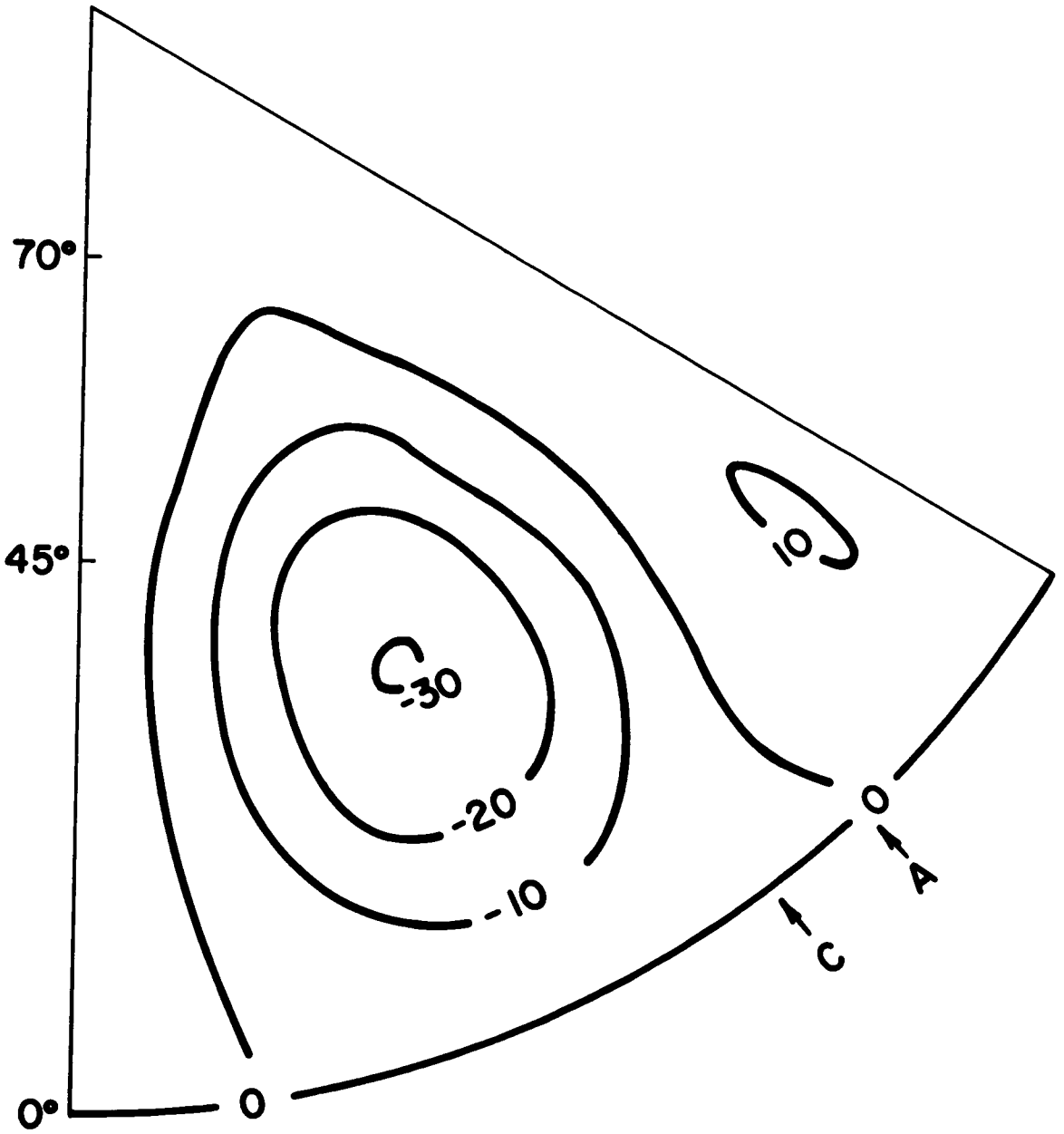

Figure 8. Same as fig. 6, but for t = 6 days.

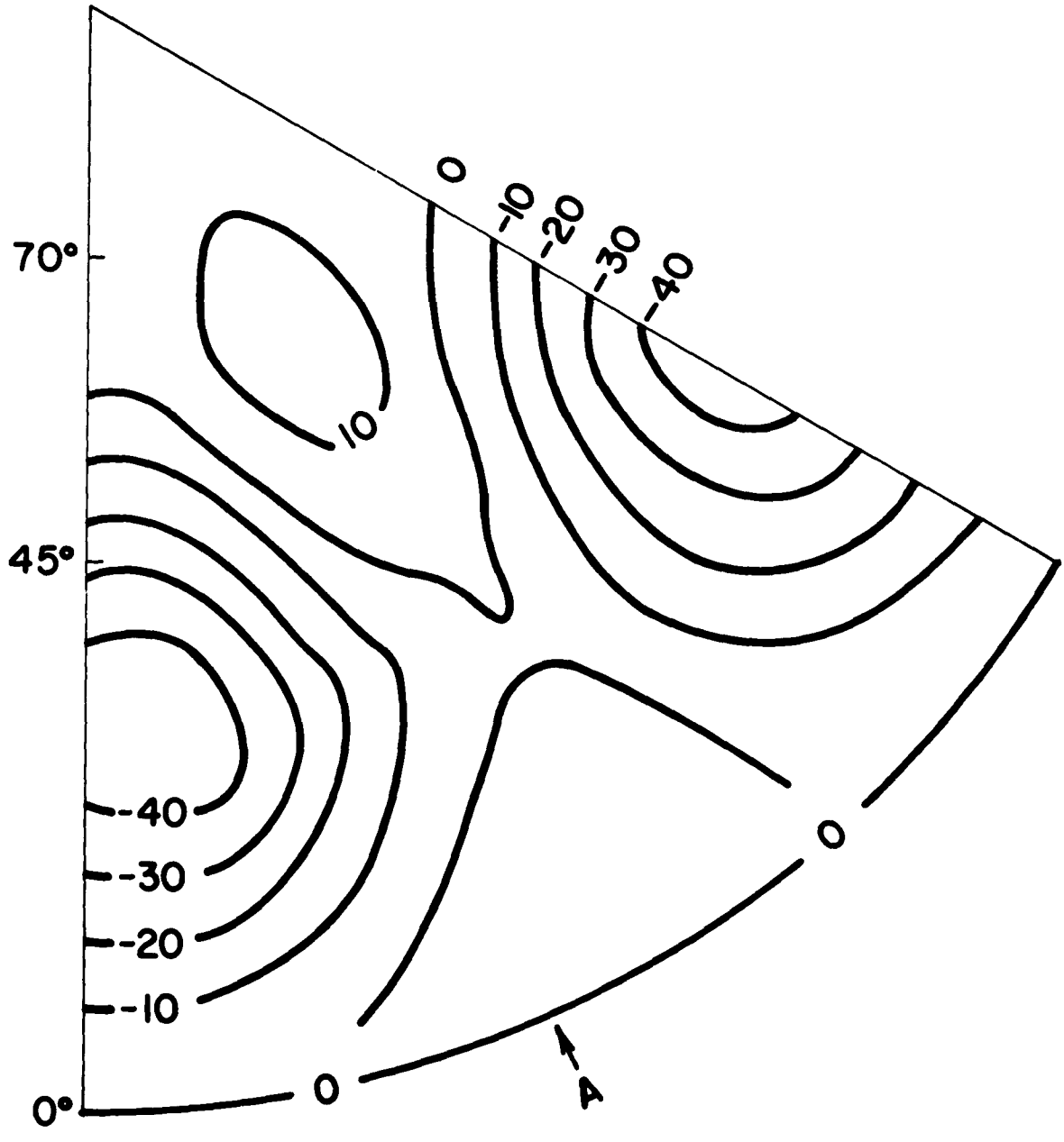

Figure 9. Same as fig. 6, but for t = 8 days.

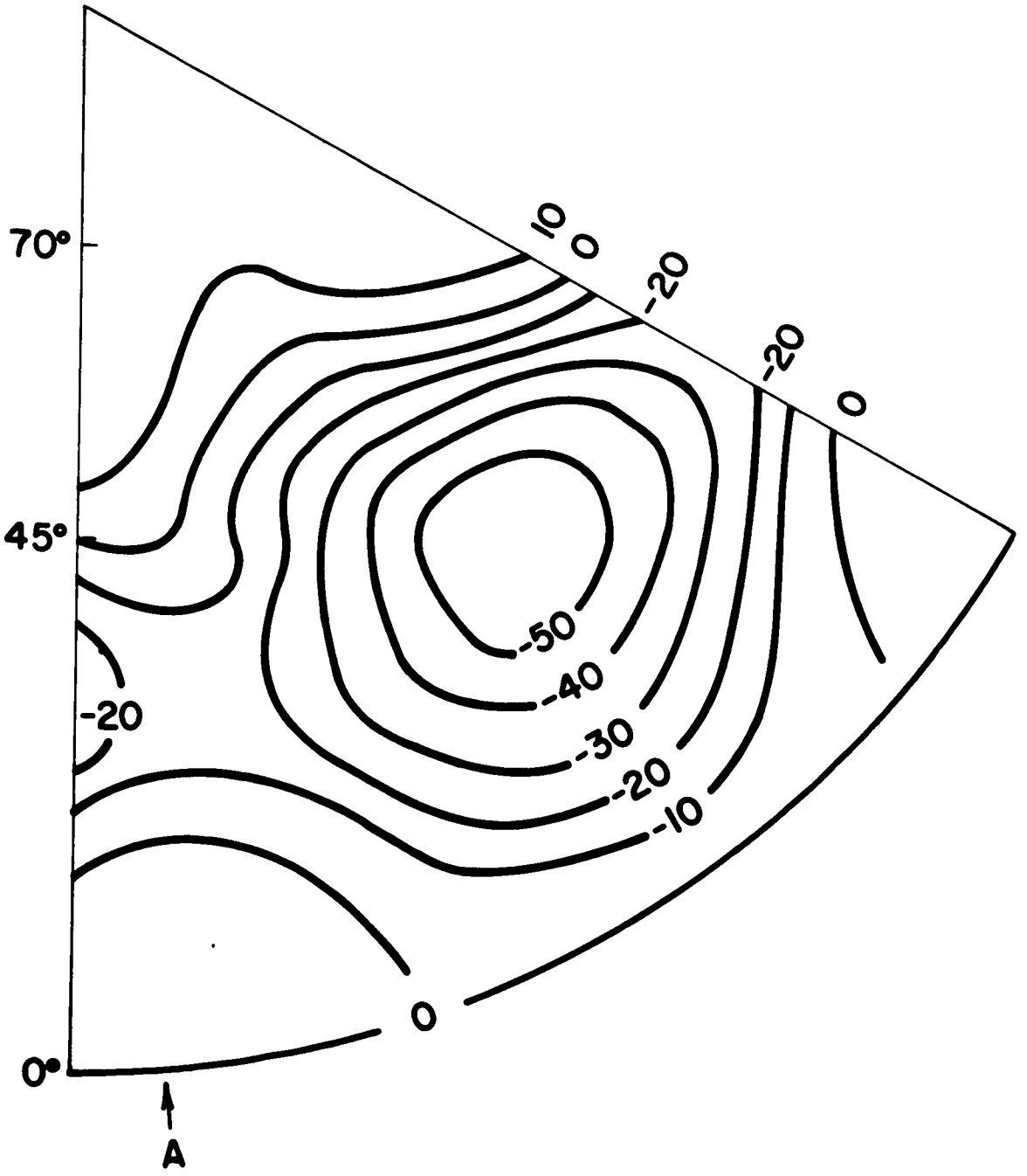

Figure 10. Same as fig. 6, but for t = 10 days.

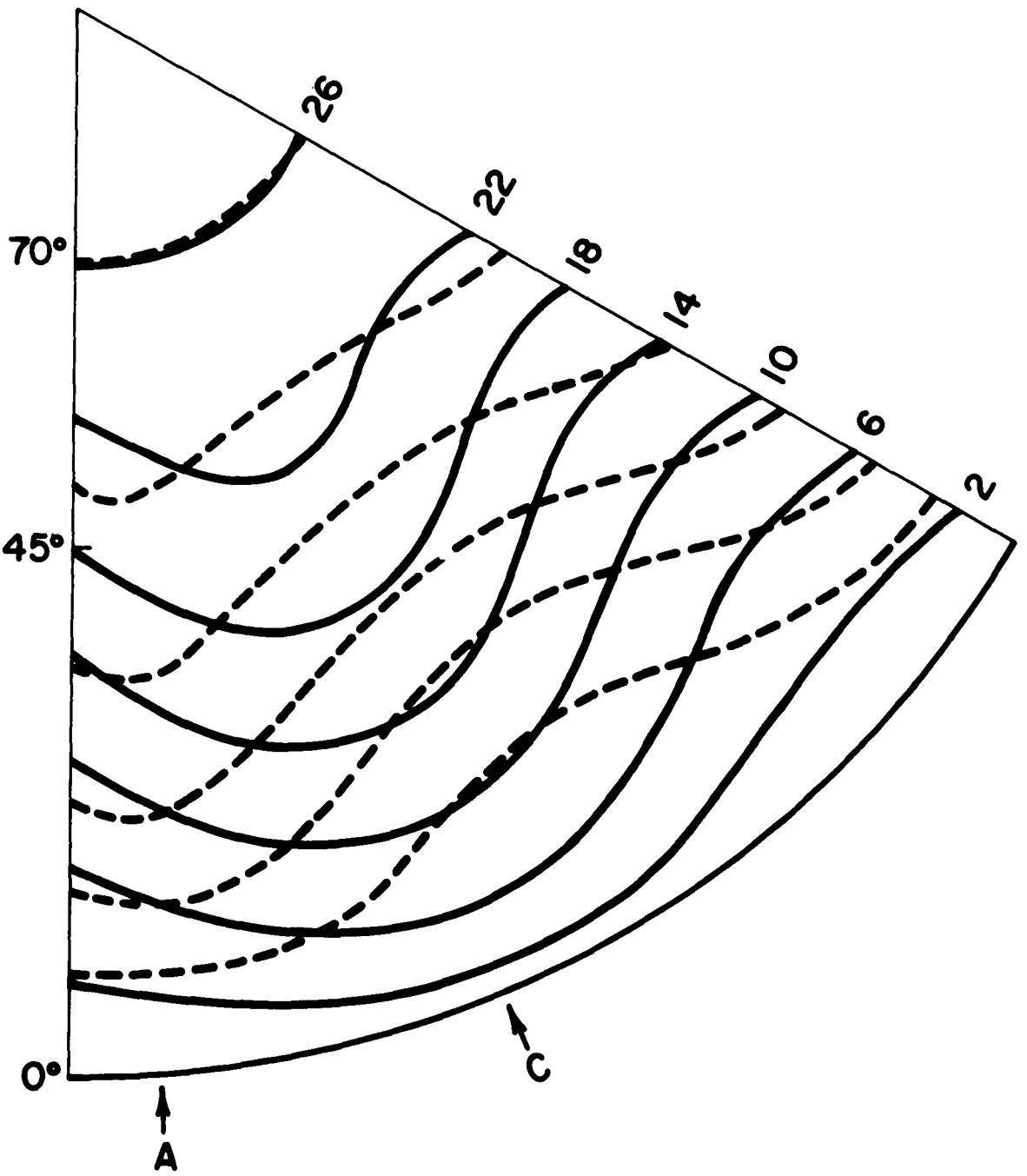

Figure 11. A sixth part of the computed stream function solution at t = 10 days with the original 10 deg grid, with α = 0.32, ϵ = 0.50 $m^2 sec^{-2}$, and Δt = 1 hr. The units are $10^7 m^2 sec^{-1}$. See fig. 1.

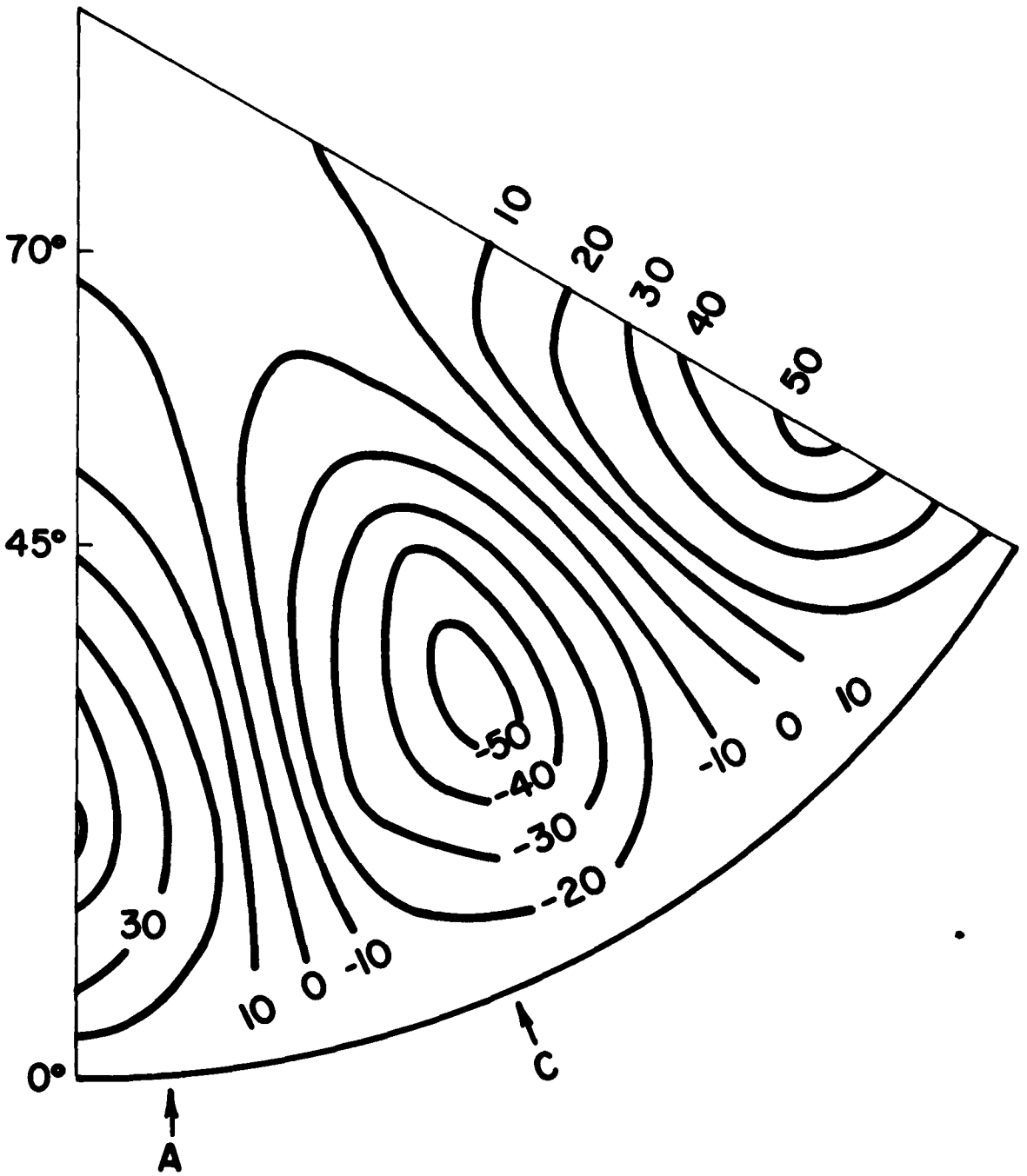

Figure 12. A sixth part of the error field of the computed stream function solution at t = 10 days with the 10 deg grid. The units are $10^6 m^2 sec^{-1}$. See fig. 1.

With the 10 deg grid (see Gates and Riegel, 1962) the wave speed in the numerical solutions is lowered to approximately 80 percent of true speed, and is further evidence of the dominant role of spatial truncation error in these calculations.

3. Extended numerical integrations with a modified grid.

In an effort to reduce this wave distortion in middle latitudes, the differencing scheme was changed such that in (3) - (5) the parameter $m = 1$ for latitudes $0 \leq \phi \leq 70$N, $m = 2$ for 75N, $m = 3$ for 80N, and $m = 6$ for 85N. The polar calculations still use only 6 of the points at 85N, forming a polar hexagonal grid. A sixth section of this modified differencing grid is shown in Fig. 13, although the full array of points for each 5 deg lat and 5 deg long continue to be carried in order to avoid interpolation (see Gates and Riegel, 1962). The values of the coefficients in (3) may readily be determined from those given earlier for the unmodified grid. Since the closest points now consulted in an application of (3), or in the determination of η, are approximately 190 km apart at 70N, the value of Δt was reduced to $\frac{1}{2}$ hr in order to avoid computational instability with the conventional centered difference scheme.

With the same analytic 6-wave initial conditions used earlier, a series of tests of the relative efficiency of various overrelaxation coefficients was made for the previously determined streamfunction tendency residue tolerance $\epsilon = 0.50$ m^2 sec^{-2}. From these tests at $t = 0$, summarized in Fig. 14 along with the corresponding data for the unmodified grid, the value $\alpha = 0.28$ was selected for use in

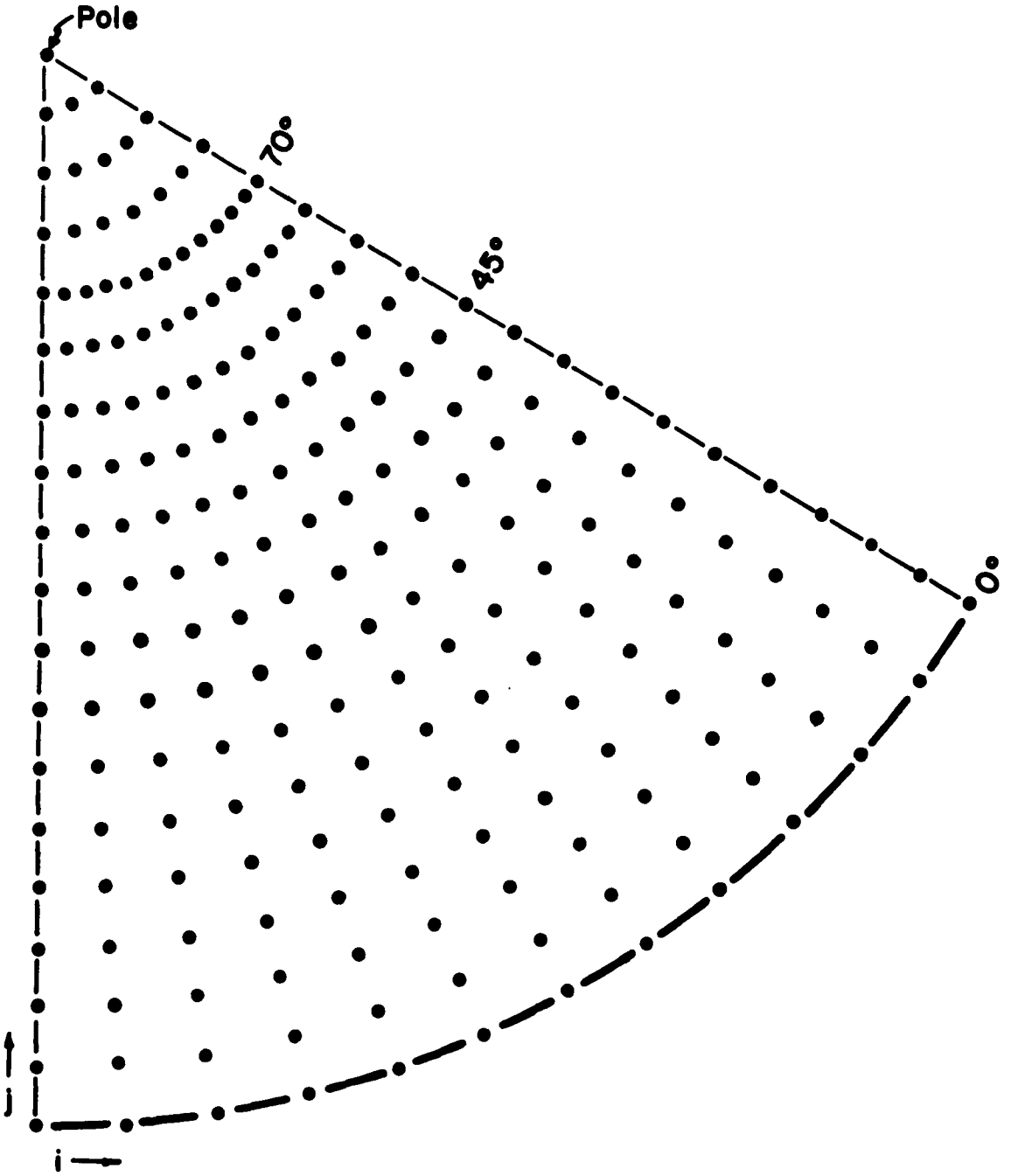

Figure 13. A sixth part of the modified 5 deg finite-difference grid.

the extended integration on the modified grid. It may be noted that the seemingly small modification of the computing scheme has had a substantial effect upon the relative efficiency of the relaxation solution. The number of scans of the grid required for convergence after the initial solution shown in Fig. 14 was approximately 15.

With the modifications described above the streamfunction integrations to t = 10 days are shown in Figs. 15-19, and the associated errors are shown in Figs. 20-24; these figures correspond to Figs. 1-10 for the original (unmodified) grid. From these figures it is at once evident that the numerical solutions obtained with the modified grid are superior: by 10 days no wave distortion is evident, and the relatively smooth error distribution reflects the systematic underestimate of the wave speed due to the dominant spatial truncation error.

4. Integration with observed atmospheric data.

The use of the spherical difference scheme with analytic data should be supplemented by an integration using observed data if the scheme's application to practical numerical weather prediction is to be examined. To this end, the 500 mb contour data for 15 GMT 18 November 1955 was selected from the U.S. Weather Bureau's Historical Map Series, and was used in the preparation of a 2-day numerical integration. The observed 500 mb contour maps for this period are shown in figs. 25-27.

Before the integration could proceed, the streamfunction ψ stipulated by the assumption of horizontal non-divergent flow first had to be determined. The pertinent equation is in this case the balance equation

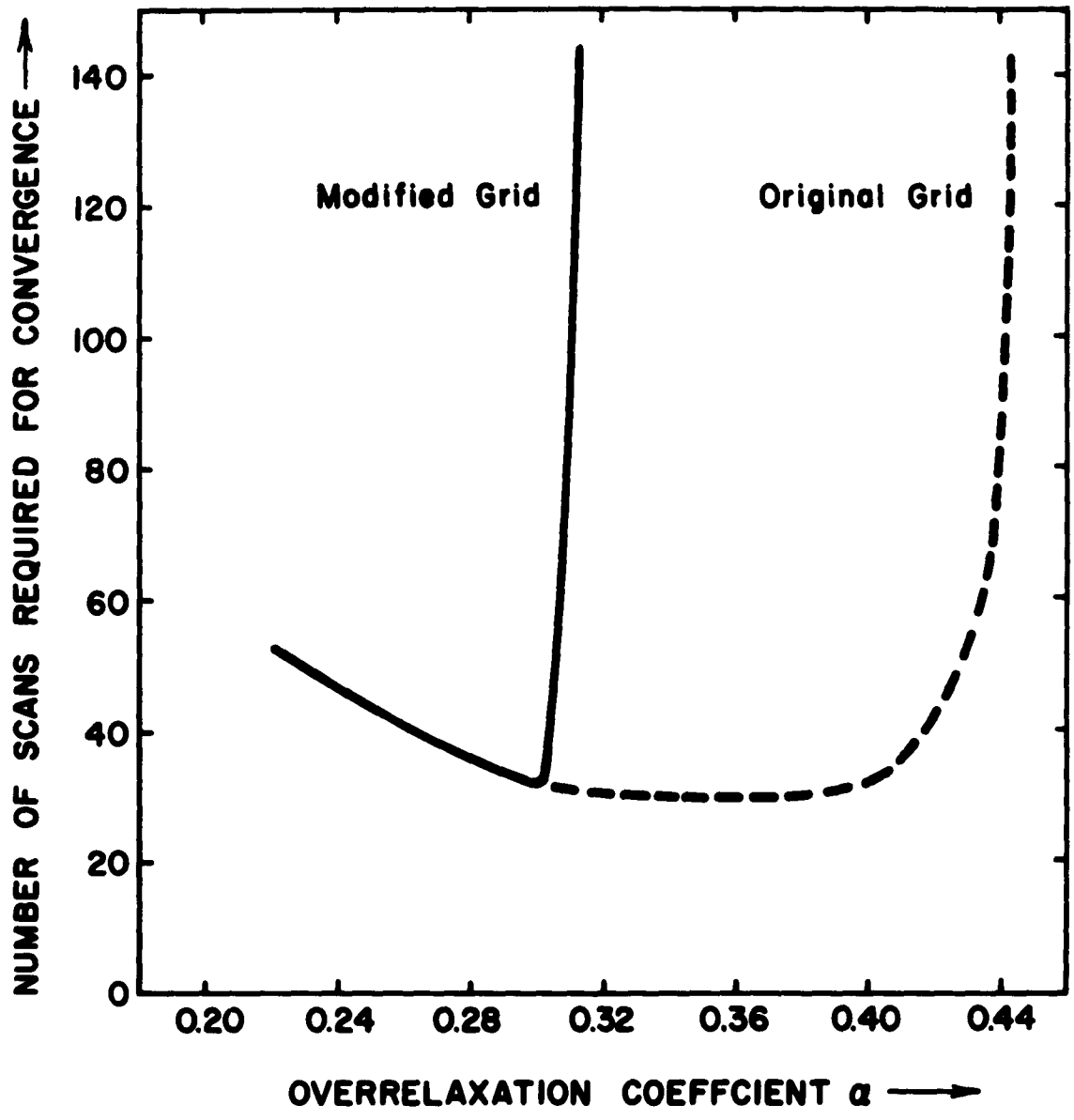

Figure 14. The scans of the 1297-point 5 deg grid required for convergence of the relaxation solution at $t = 0$, as a function of the overrelaxation coefficient α with $\epsilon = 0.50\ m^2 sec^{-2}$. The original grid is that shown in Gates and Riegel (1962); the modified grid is that shown in fig. 13.

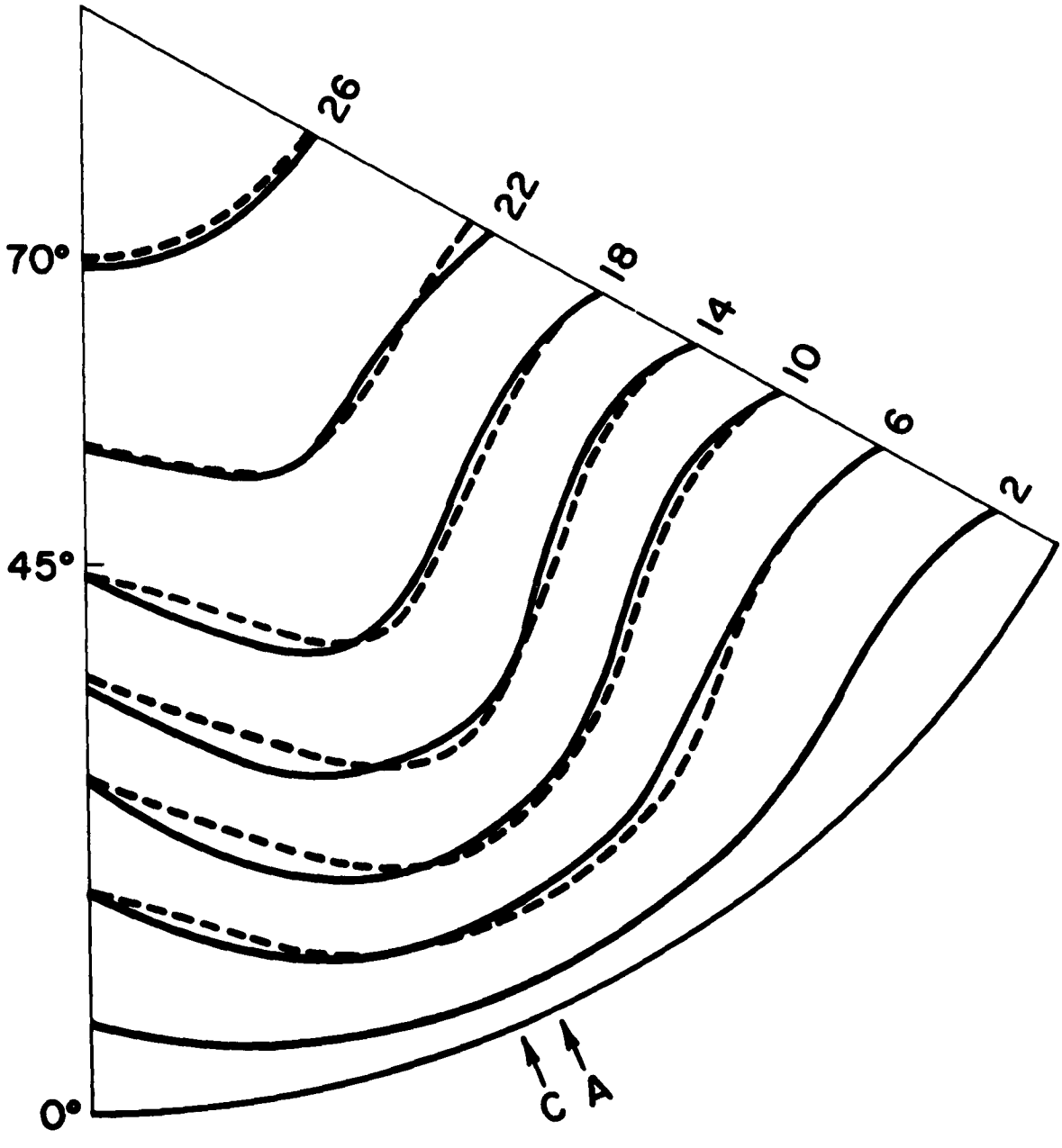

Figure 15. A sixth part of the computed stream function solution at t = 2 days with the modified 5 deg grid (see fig. 13), with α = 0.28, ϵ = 0.50 $m^2 sec^{-2}$, and Δt = ½ hr. The dashed lines are the corresponding analytic solution. The units are $10^7 m^2 sec^{-1}$, and the arrows "A" and "C" indicate the positions of the analytic and computed stream function troughs, respectively. All stream function values are negative.

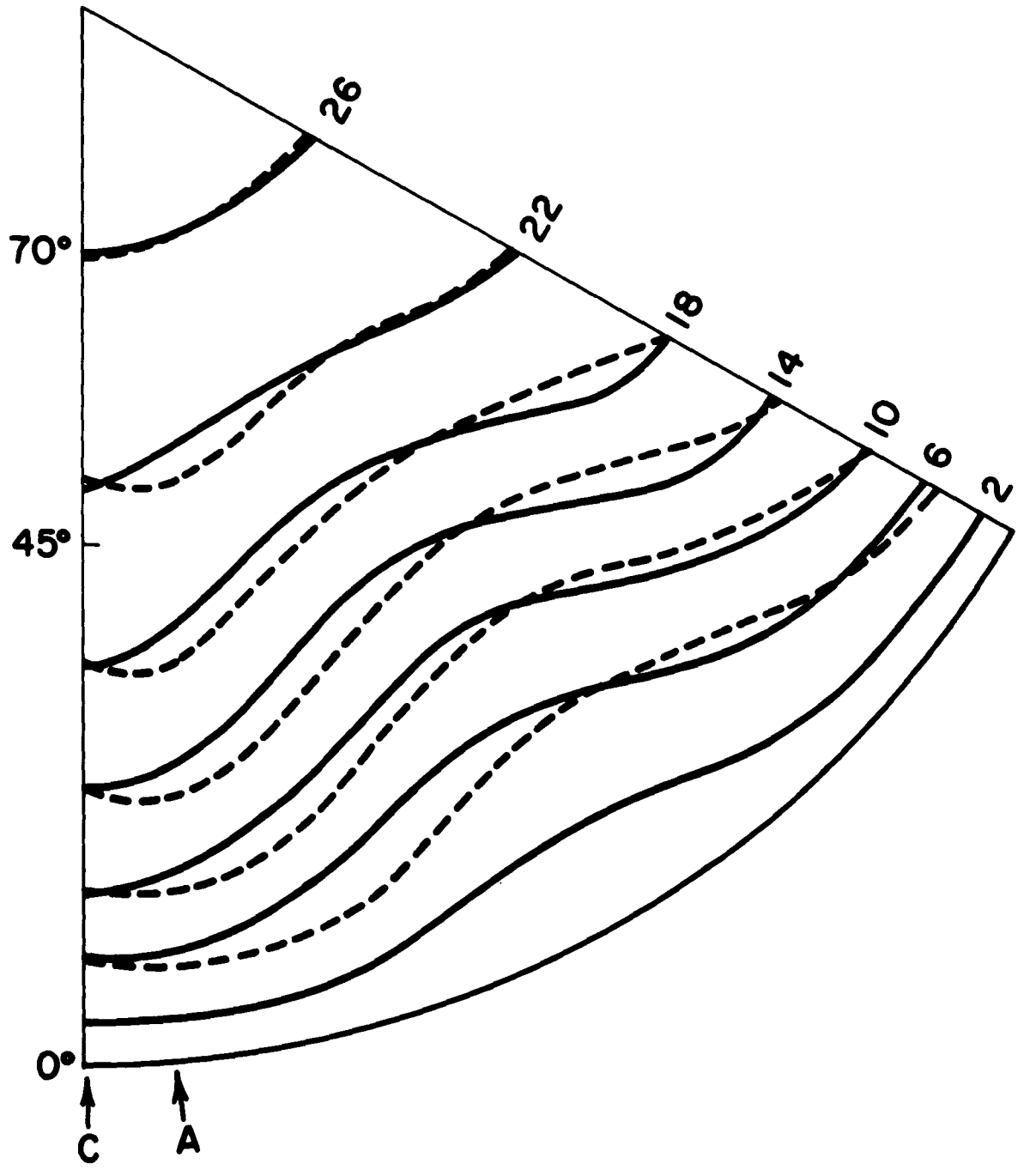

Figure 16. Same as fig. 15, but for t = 4 days.

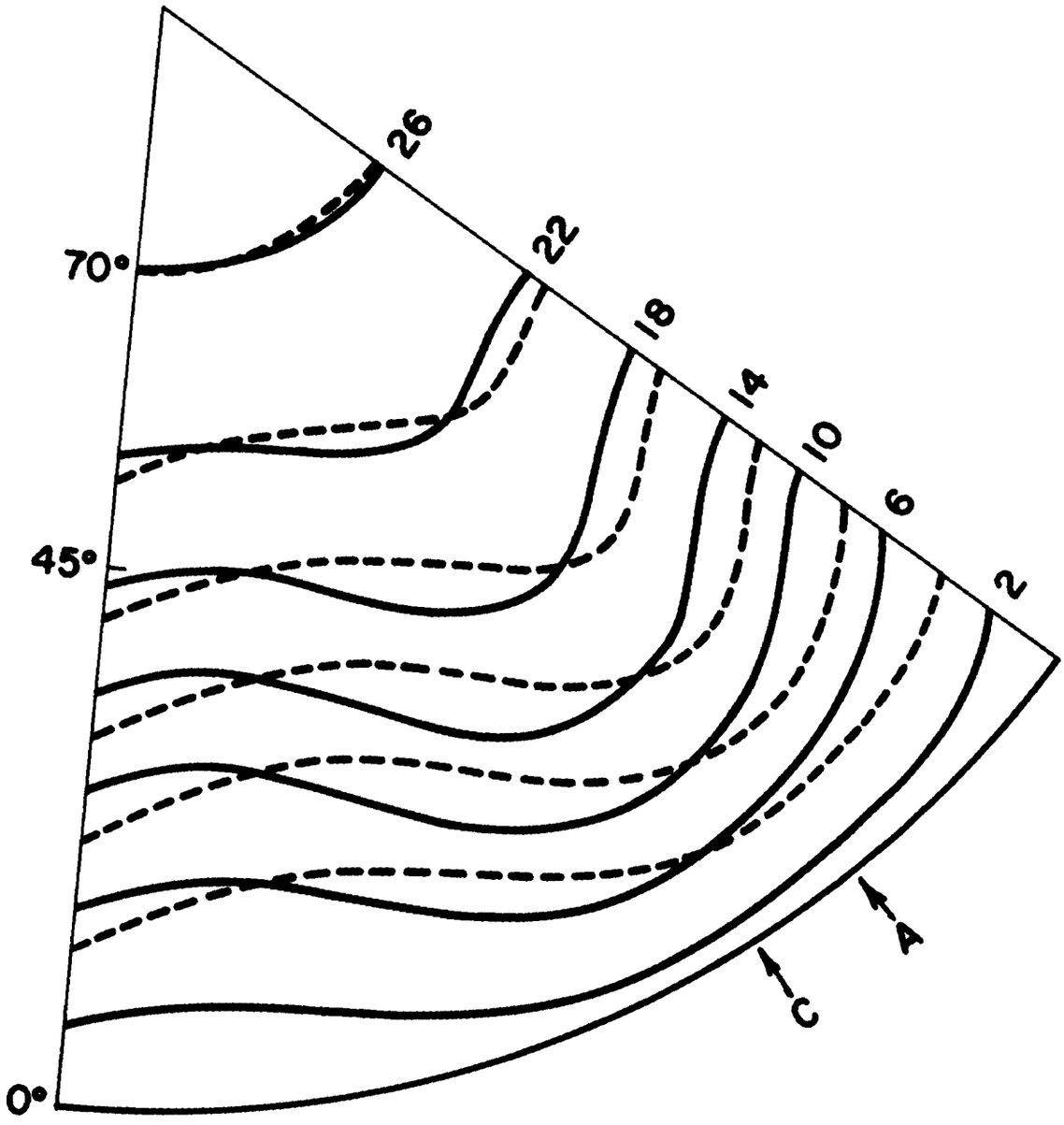

Figure 17. Same as fig. 15, but for t = 6 days.

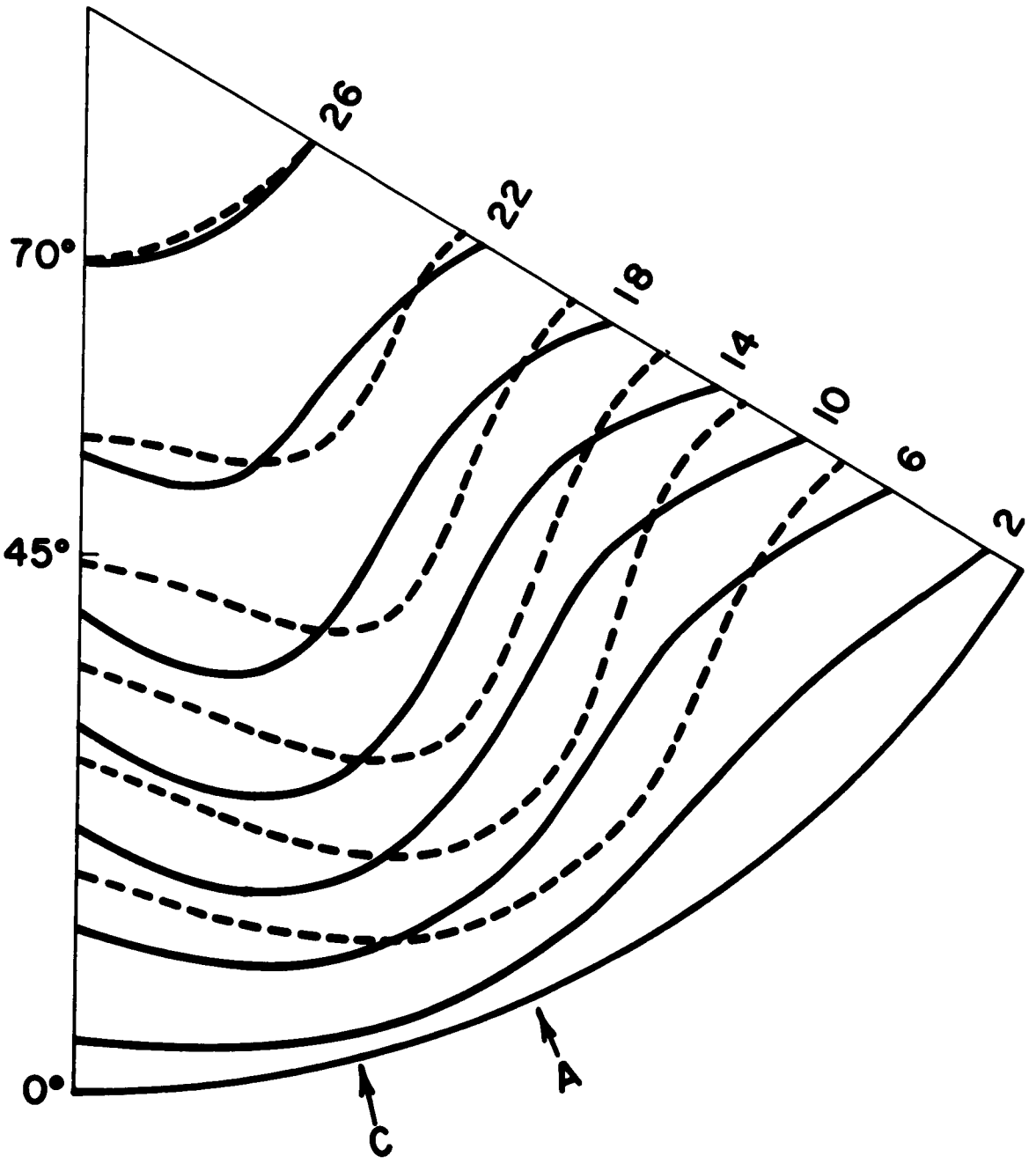

Figure 18. Same as fig. 15, but for t = 8 days.

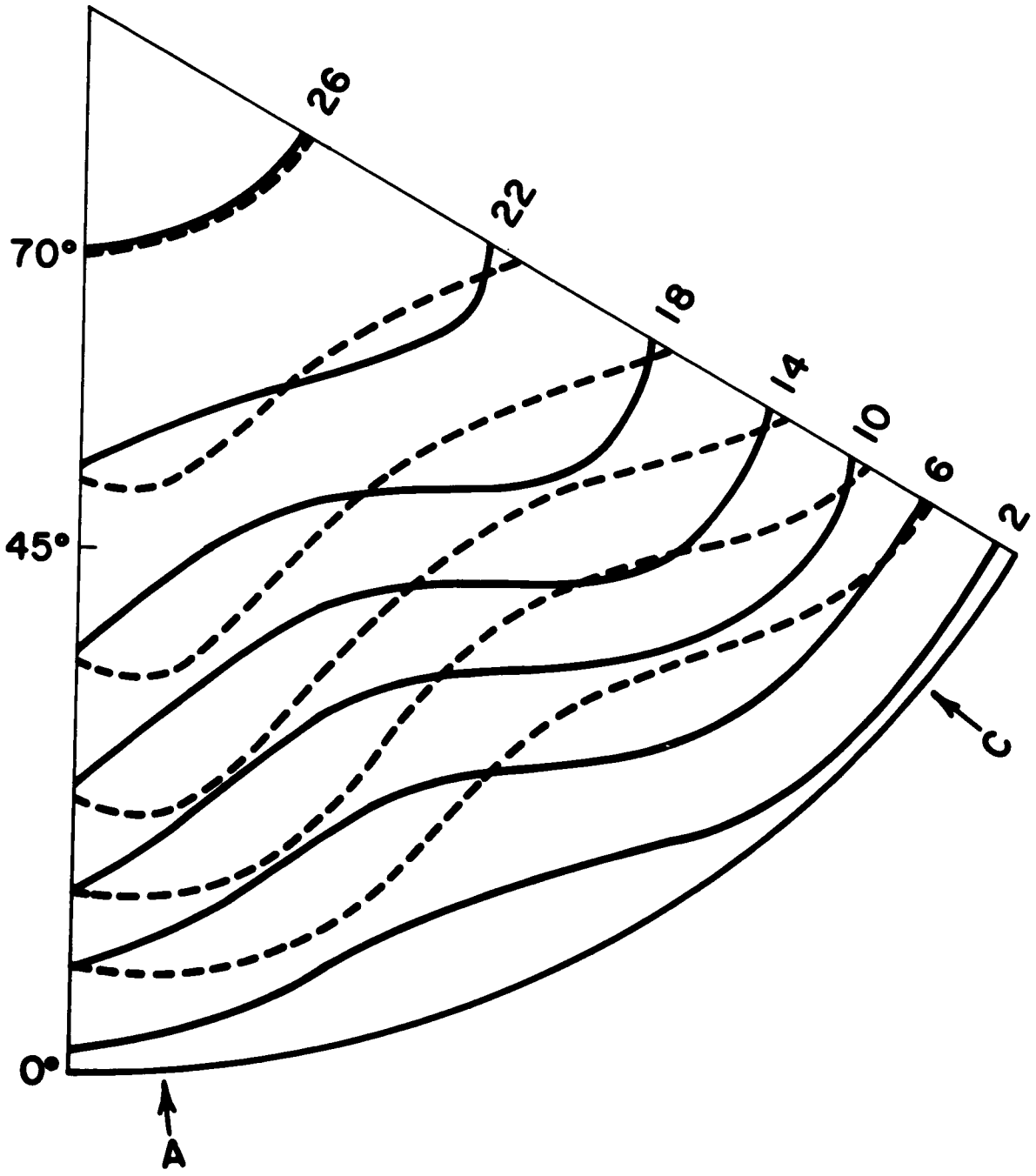

Figure 19. Same as fig. 15, but for t = 10 days.

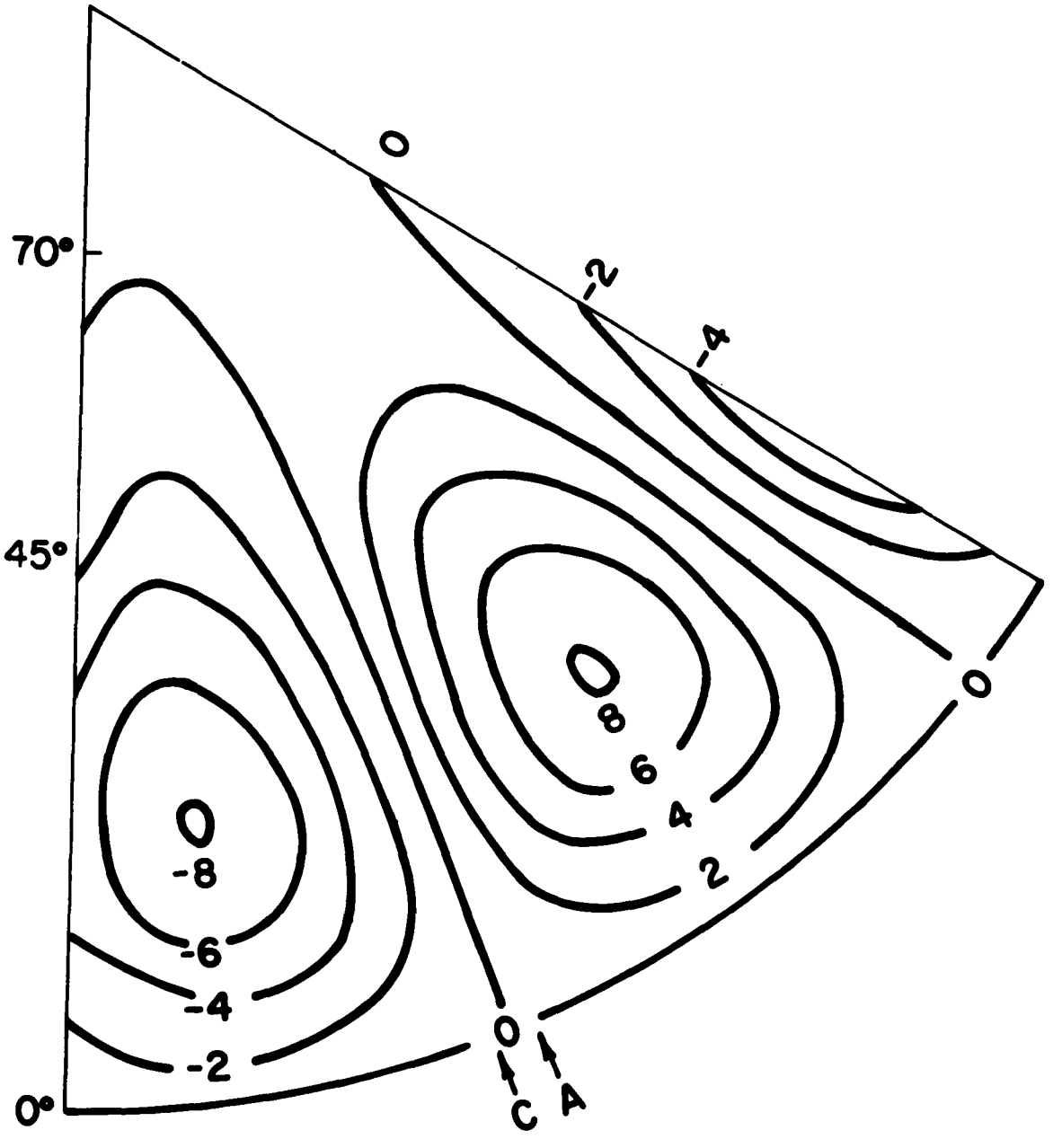

Figure 20. A sixth part of the error field of the computed stream function solution at t = 2 days with the modified 5 deg grid. The units are $10^6 m^2 sec^{-1}$. See fig. 15.

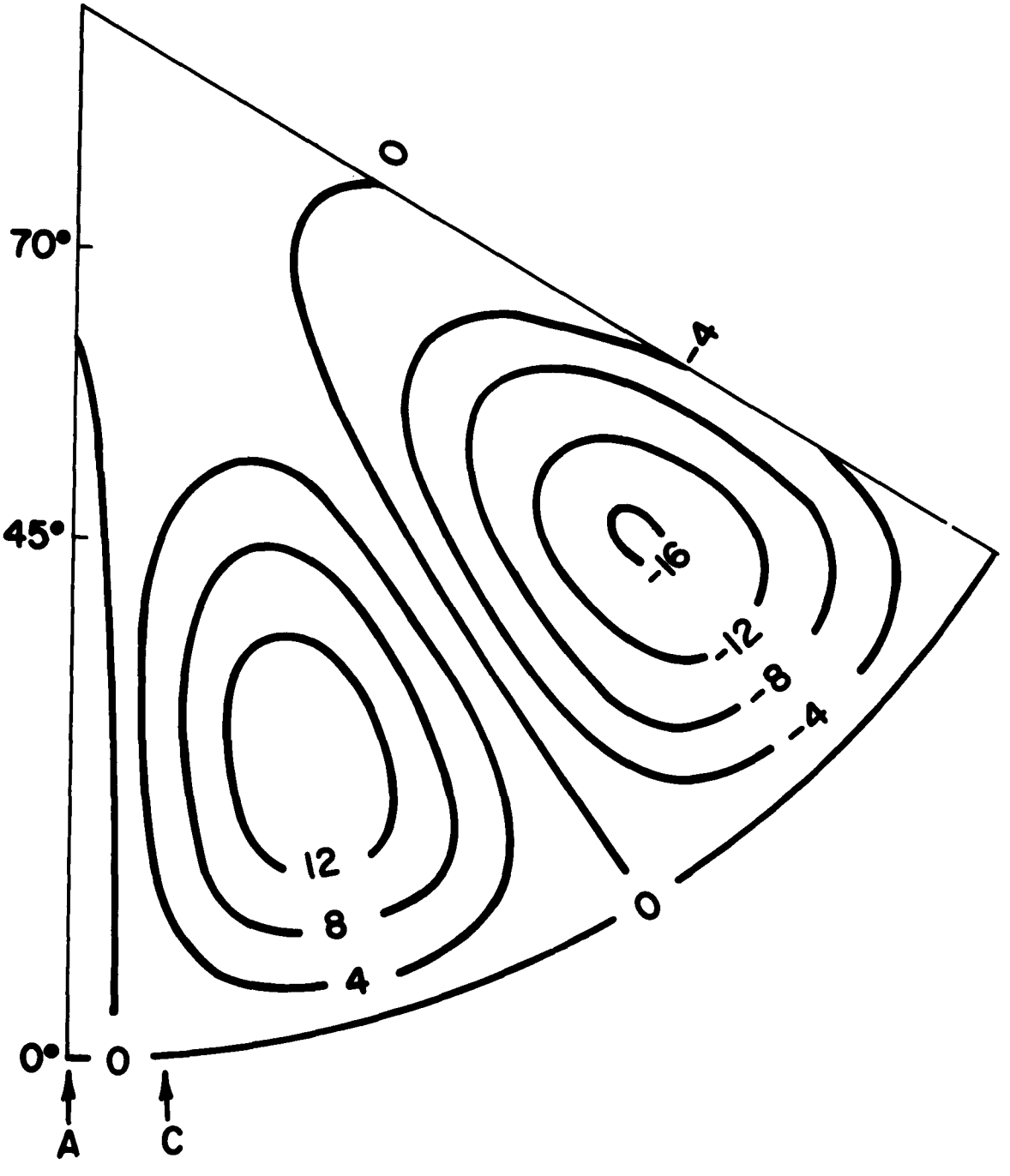

Figure 21. Same as fig. 20, but for t = 4 days.

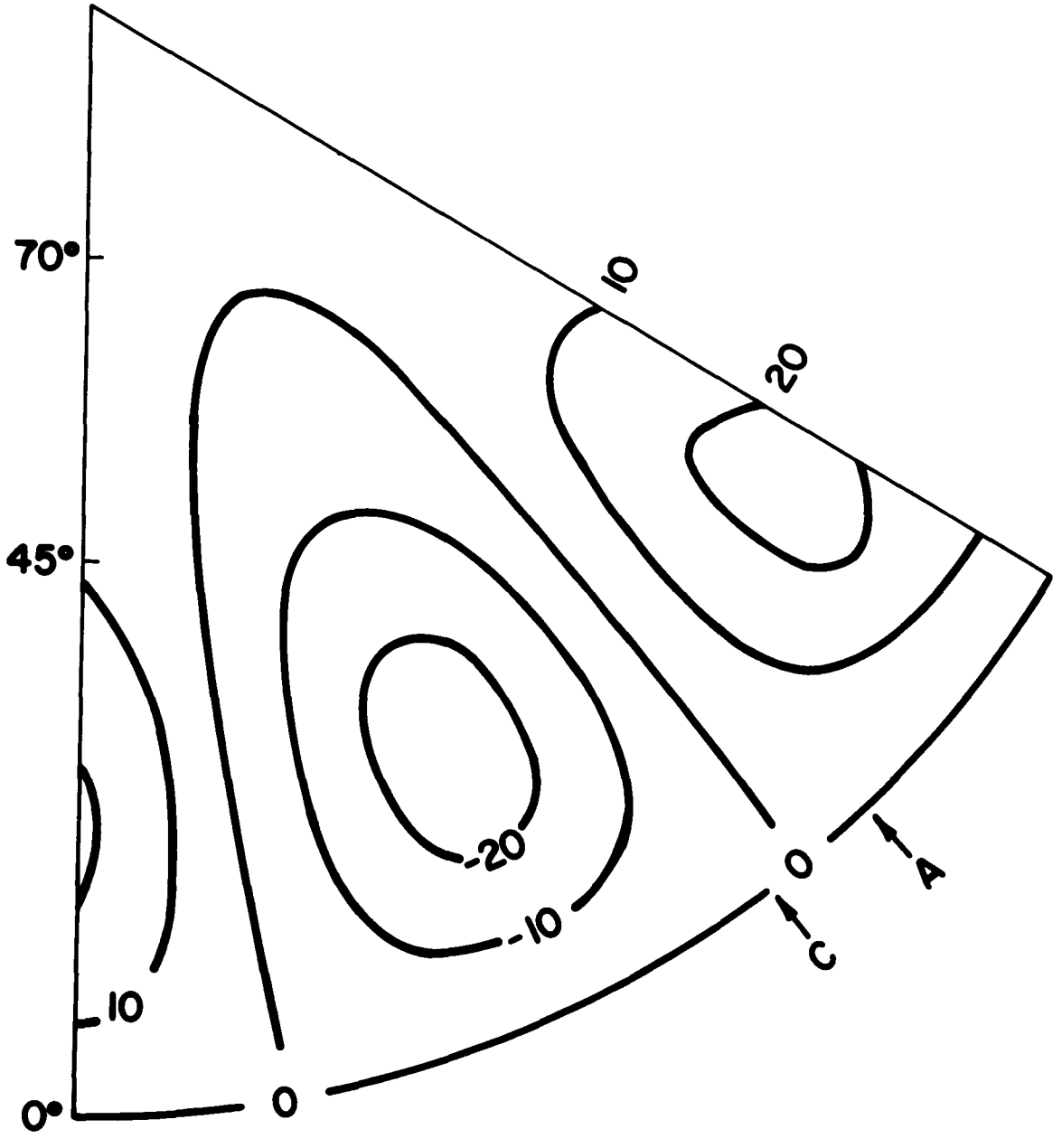

Figure 22. Same as fig. 20, but for t = 6 days.

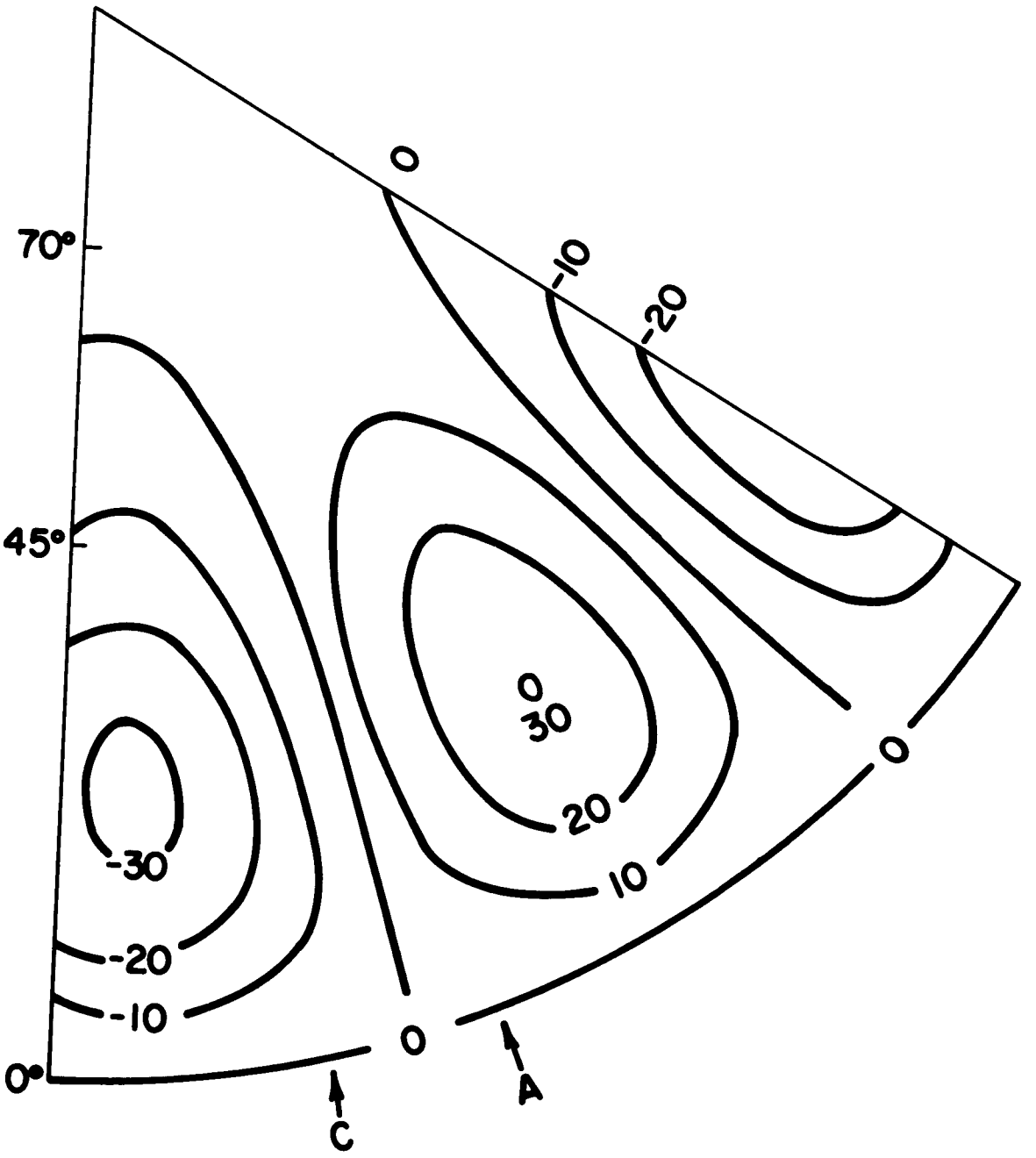

Figure 23. Same as fig. 20, but for t = 8 days.

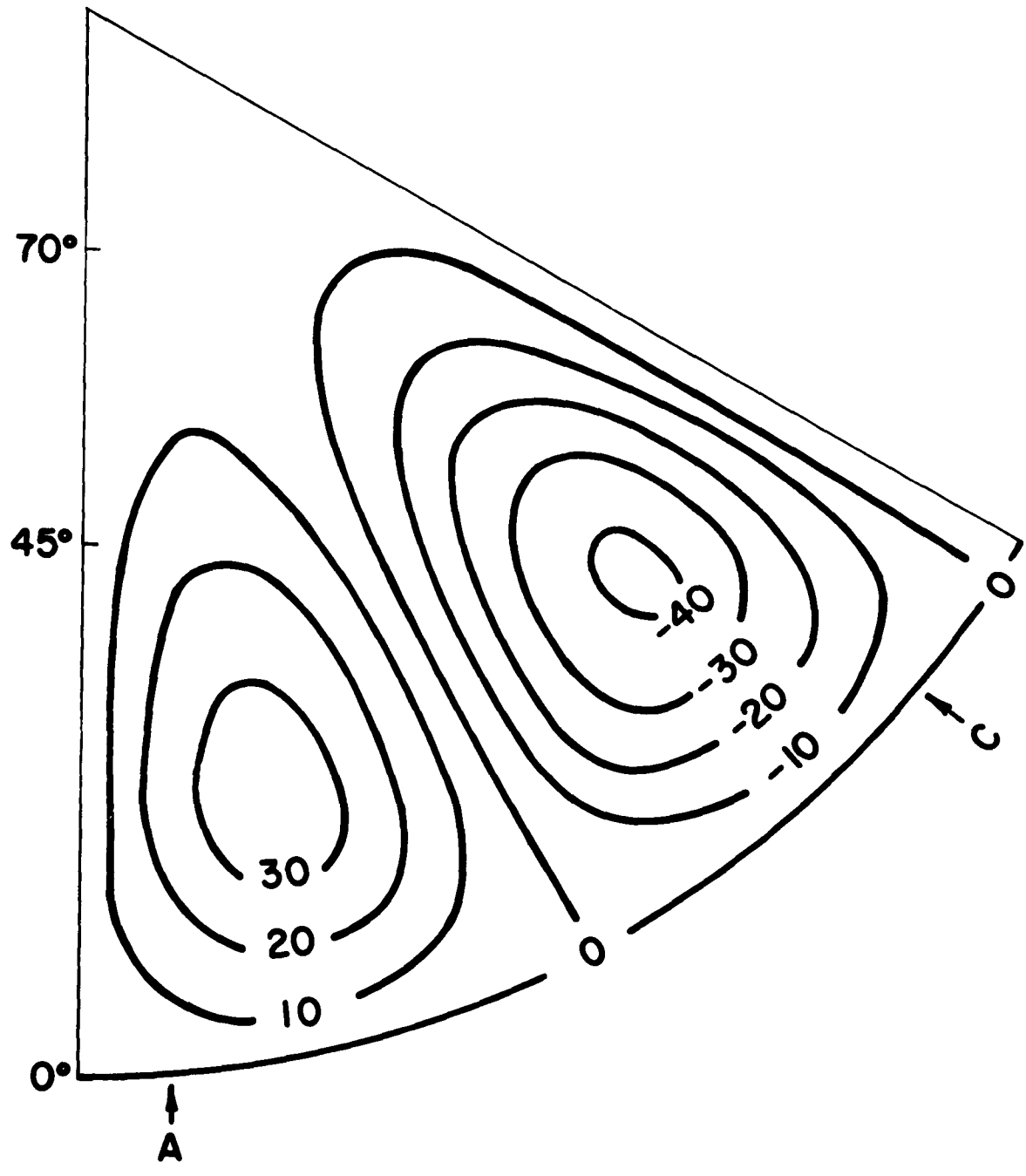

Figure 24. Same as fig. 20, but for t = 10 days.

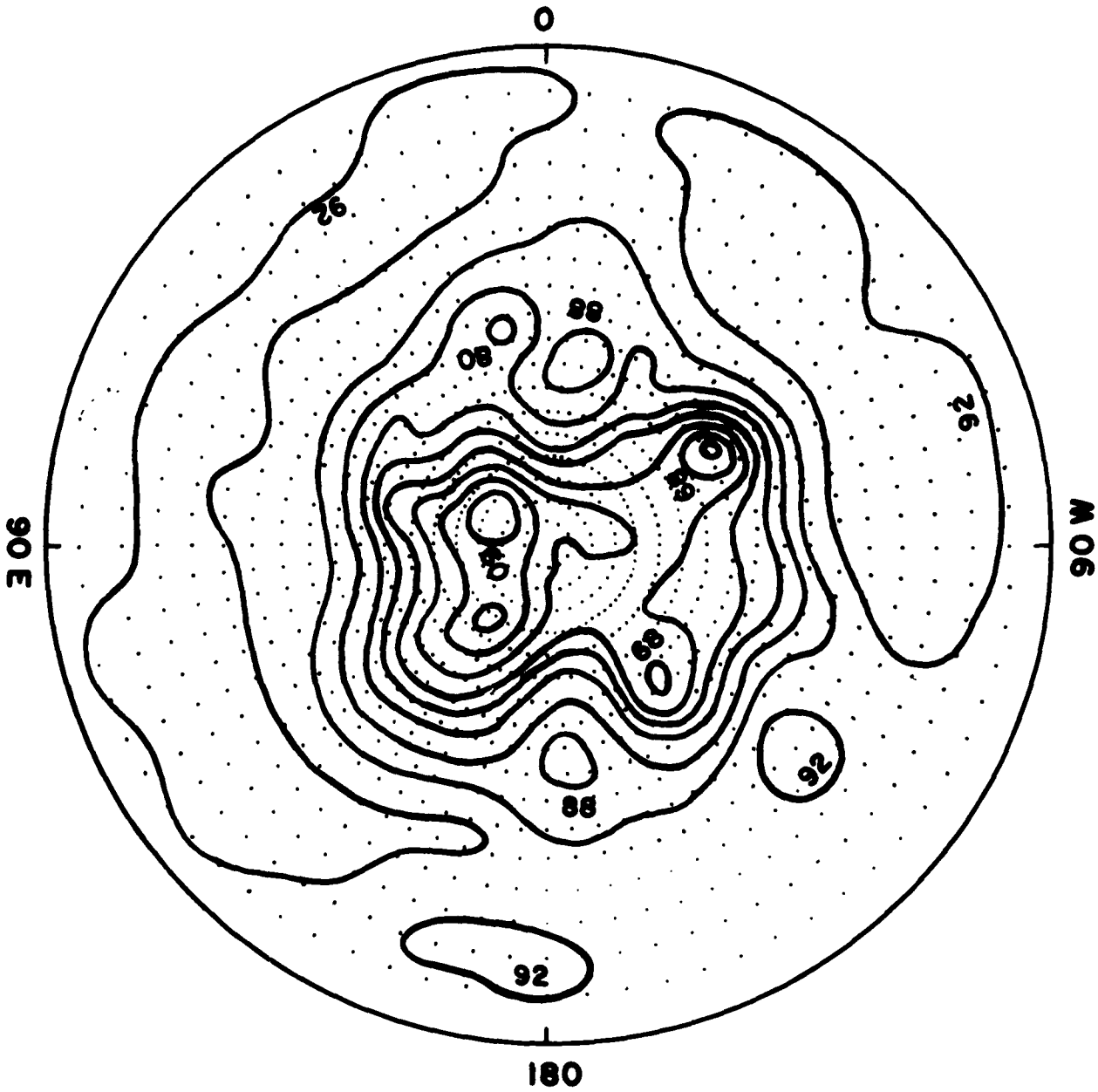

Figure 25. The observed 500 mb topography on 1500 GMT, 18 November, 1955. The contours are drawn each 400 ft.

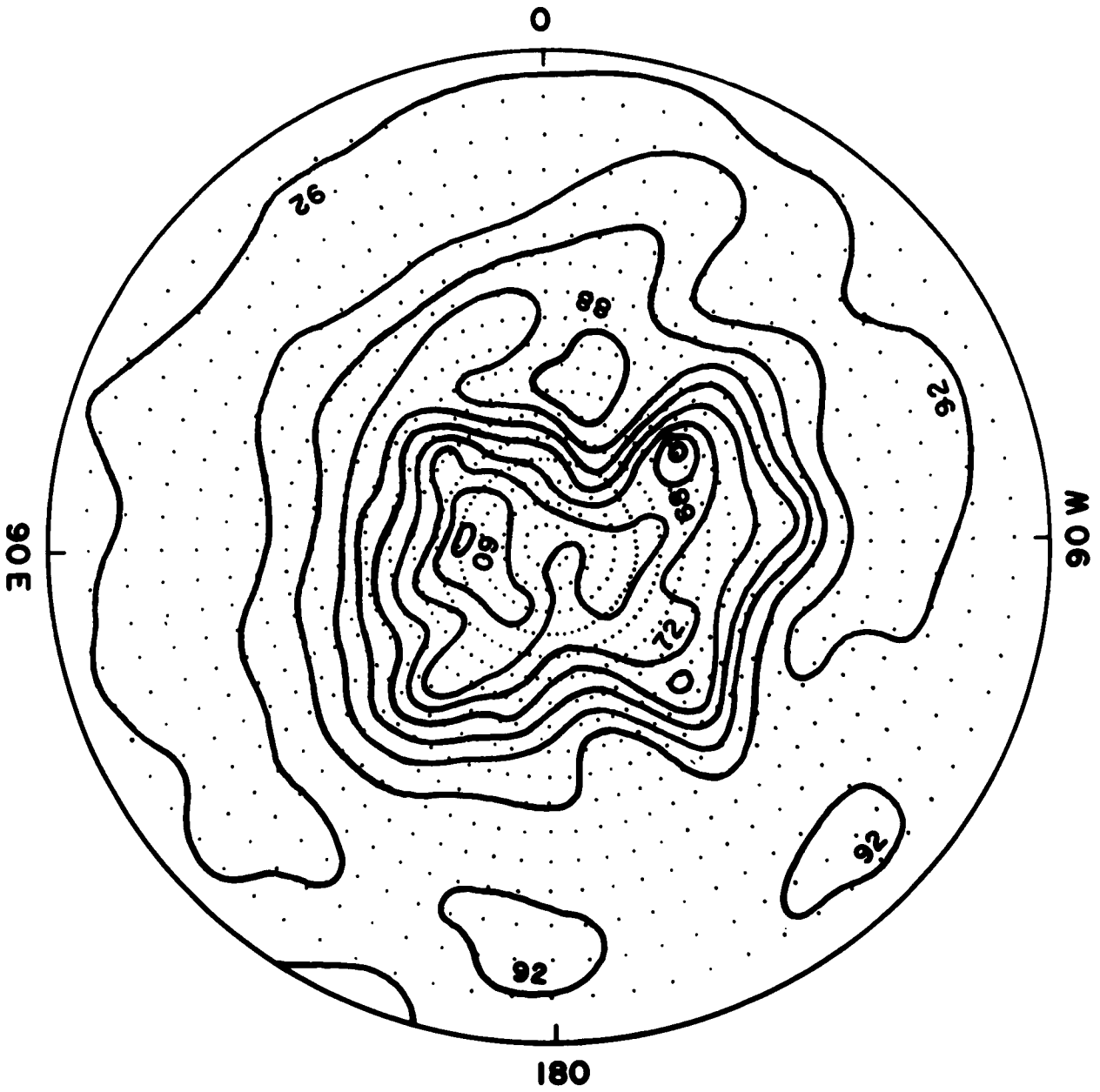

Figure 26. The observed 500 mb topography on 1500 GMT, 19 November 1955.

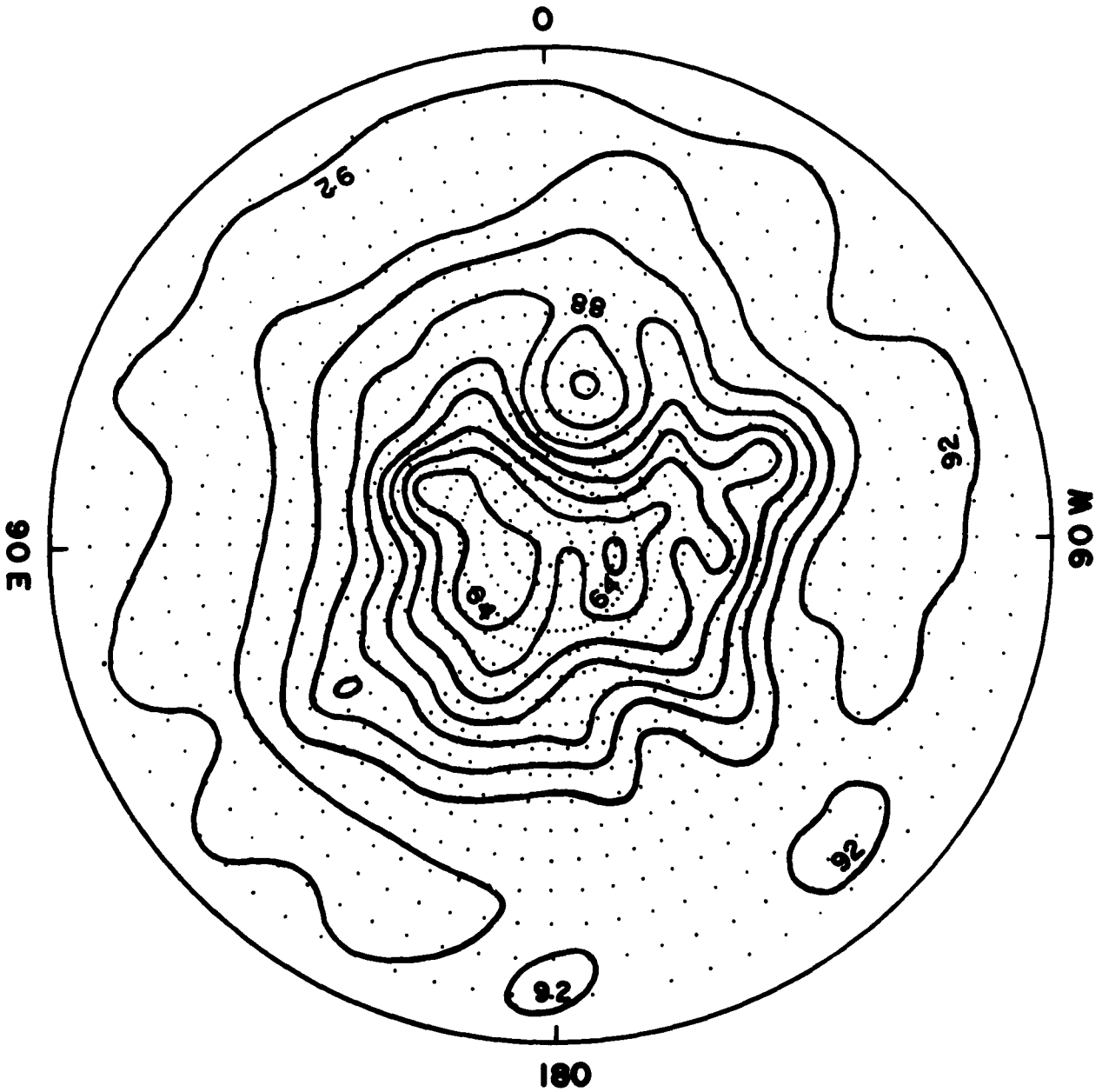

Figure 27. The observed 500 mb topography on 1500 GMT, 20 November 1955.

$$\nabla \cdot (f \nabla \psi) - g \nabla^2 z + 2 \left[\frac{\partial^2 \psi}{\partial x^2} \frac{\partial^2 \psi}{\partial y^2} - \left(\frac{\partial^2 \psi}{\partial x \partial y} \right)^2 \right] = 0 \ , \tag{6}$$

written here for convenience in rectangular coordinates. In a number of studies of the use of this equation at 500 mb, the non-linear terms have been found to contribute relatively little to the stream-function solution with observed contour heights. For the present purposes it therefore seems sufficient to use the linearized version of (6), which in spherical coordinates becomes

$$\frac{f}{g} \left[\frac{1}{r^2 \cos\phi} \frac{\partial}{\partial \phi} \left(\cos\phi \frac{\partial \psi}{\partial \phi} \right) + \frac{1}{r^2 \cos^2\phi} \frac{\partial^2 \psi}{\partial \lambda^2} \right] + \frac{\beta}{g r} \frac{\partial \psi}{\partial \phi}$$

$$= \frac{1}{r^2 \cos\phi} \frac{\partial}{\partial \phi} \left(\cos\phi \frac{\partial z}{\partial \phi} \right) + \frac{1}{r^2 \cos^2\phi} \frac{\partial^2 z}{\partial \lambda^2} \ . \tag{7}$$

The introduction of centered finite differences on the modified 5 deg grid of § 3 leads to the difference equation approximating (7) in the form

$$(h_1 - h_2 + h_3) \psi_{ij+1} + (h_1 + h_2 - h_3) \psi_{ij-1} + h_1^{-1} (\psi_{i+m_j} + \psi_{i-m_j})$$

$$- (2h_1 + 2h_1^{-1}) \psi_{ij} = \frac{g}{2f_j} \left[(h_1 - h_2) z_{ij+1} + (h_1 + h_2) z_{ij-1} \right.$$

$$\left. + h_1^{-1} (z_{i+m_j} + z_{i-m_j}) - (2h_1 + 2h_1^{-1}) z_{ij} \right] \ , \tag{8}$$

where h_1 and h_2 are given by (4) and (5), and where

$$h_3 = h_1 r \Delta\phi \, (2f_j)^{-1} \beta_j \ , \tag{9}$$

with f_j the Coriolis parameter, β_j the Rossby parameter, and the remaining symbols as previously defined. At the pole the linear

portion of (6) is approximated on a locally hexagonal grid as

$$\psi_1+\psi_2+\psi_3+\psi_4+\psi_5+\psi_6-6\psi_P = \frac{g}{2f_P}\left(z_1+z_2+z_3+z_4+z_5+z_6-6z_P\right), \quad (10)$$

where the subscripts 1 to 6 denote 6 equally-spaced points at 85°N, and the subscript P denotes the pole.

Starting from the known z, equations (8) and (10) were solved for the streamfunction ψ by extrapolated Liebmann relaxation, using $\psi = 0$ as a boundary condition at the equator. A series of tests for various values of the overrelaxation coefficient and residue tolerance were made, and are shown in fig. 28. The solution with $\epsilon = 0.1 \times 10^5$ m^2 sec^{-1} and $\alpha = 0.29$ was ultimately selected, although there was very little variation in the solutions with α for this value of ϵ. We may note the similarity of the useful α range here with that in fig. 14, and conclude that the n_3 term in (8) has caused no difficulty in the relaxation solution. The relaxation solutions of (3) itself, once ψ had been found, required approximately 110 scans per ($\frac{1}{2}$ hr) time step, with the values $\alpha = 0.30$ and $\epsilon = 0.05$ m^2 sec^{-2}; these constants were selected from the data of fig. 14, although ϵ was here lowered by a factor of 10 in the interests of accuracy.

In order to verify the numerical integrations for ψ, (8) and (10) were rewritten for z in terms of ψ, and again solved by the relaxation method. In these inversions the overrelaxation coefficient and the residue tolerance were given the values $\alpha = 0.29$ and $\epsilon = 0.5$ ft, respectively, and required approximately 590 scans for convergence. The initially observed zonally averaged contour height at the equator was used as an equatorial boundary condition.

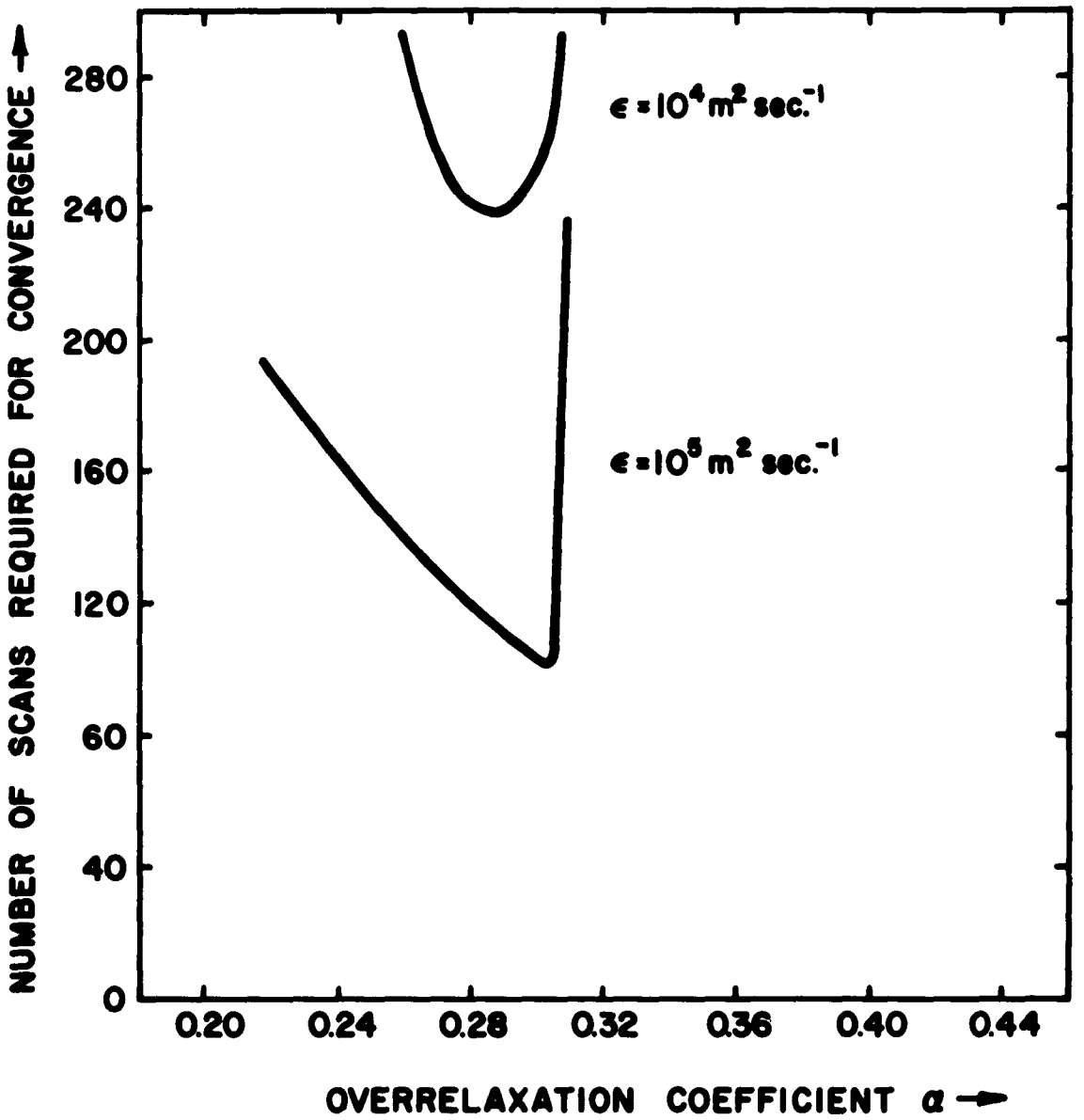

Figure 28. The scans of the 1297-point modified 5 deg grid required for convergence of the relaxation solution for ψ (actual atmospheric 500 mb data of 1500 GMT, 18 November 1955).

The forecast 500 mb contour maps computed in this manner from the 1- and 2-day numerical integrations of (3) with the modified grid are shown in figs. 29 and 30. These forecasts are not of high meteorological accuracy in that the behavior of a number of major wave systems over the hemisphere is not well predicted. An independent integration (not shown), with the same initial and boundary conditions on a conventional rectangular grid system of comparable middle-latitude resolution, was physically inadequate in the same instances, however, so that these failings may be attributed to the non-divergent barotropic model rather than to the grid scheme itself.

5. Conclusions.

In using a spherical grid scheme with changing longitudinal mesh size (Gates and Riegel, 1962), it appears important to avoid an abrupt change of mesh size in those latitudes at which large gradients characteristically occur. The latitude 70°N appears suitable for a first doubling of a 5° longitude mesh size for typical atmospheric flow at 500 mb, and this spherical grid appears to yield a smooth and well-behaved solution over the hemisphere. It is felt that such a scheme may prove of considerable use in global numerical weather prediction in which artificial lateral boundaries or overlapping rectangular grids are not desirable.

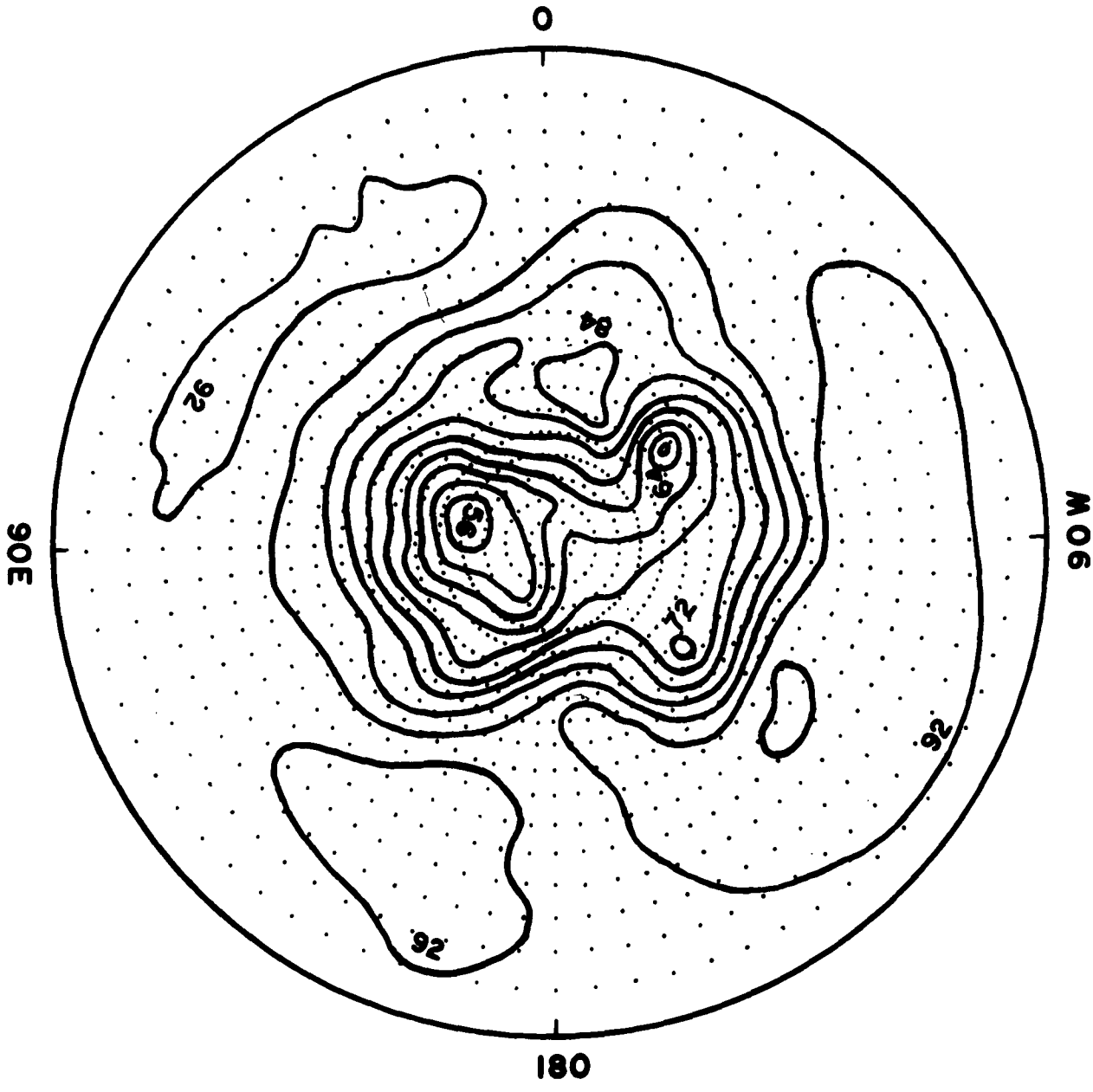

Figure 29. The forecast 500 mb topography for 1500 GMT, 19 November 1955. The initial data was that of fig. 25 (24-hr. forecast).

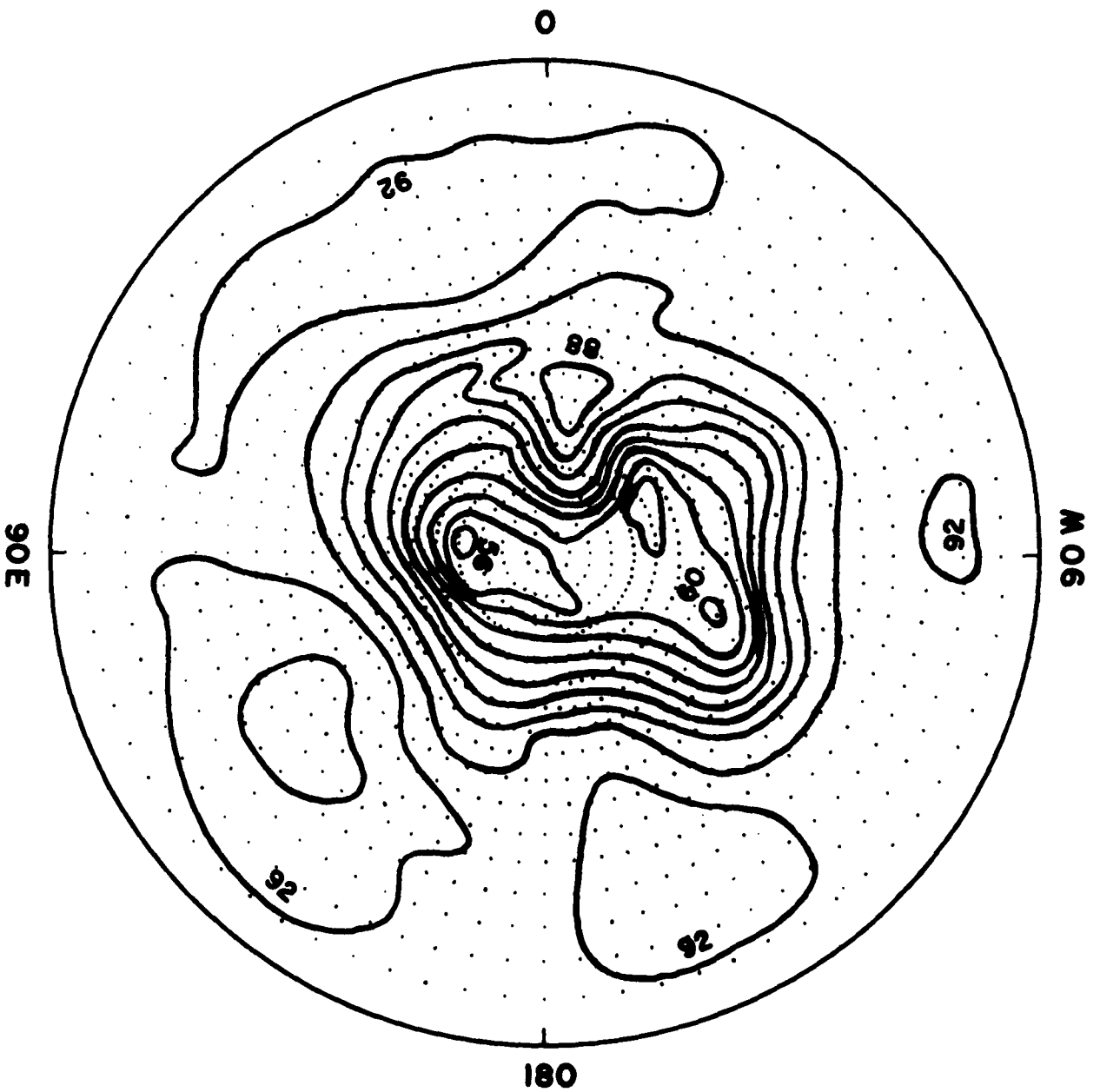

Figure 30. The forecast 500 mb topography for 1500 GMT 20 November 1955. The initial data was that of fig. 25 (48-hr forecast).

REFERENCE

Cates, W. L. and C. A. Riegel, 1962: A study of numerical errors in the integration of barotropic flow on a spherical grid, J. Geophys. Res., 67: 773-784.